BIOACTIVITY ANALYSIS OF NOVEL INDOLE DERIVATIVES ON HEPATOCELLULAR CARCINOMA AS SIRTUIN INHIBITORS

A THESIS SUBMITTED TO
THE GRADUATE SCHOOL OF NATURAL AND APPLIED SCIENCES
OF
MIDDLE EAST TECHNICAL UNIVERSITY

BY

BÜŞRA BINARCI

IN PARTIAL FULFILLMENT OF THE REQUIREMENTS
FOR
THE DEGREE OF MASTER OF SCIENCE
IN
MOLECULAR BIOLOGY AND GENETICS

SEPTEMBER 2021

Approval of the thesis:

BIOACTIVITY ANALYSIS OF NOVEL INDOLE DERIVATIVES ON HEPATOCELLULAR CARCINOMA AS SIRTUIN INHIBITORS

submitted by **BÜŞRA BINARCI** in partial fulfillment of the requirements for the degree of **Master of Science** i**n Molecular Biology and Genetics, Middle East Technical University** by,

Prof. Dr. Halil Kalıpçılar
Dean, Graduate School of **Natural and Applied Sciences** _____

Prof. Dr. Ayşe Gül Gözen
Head of Department, **Biology, METU** _____

Prof. Dr. Mesut Muyan
Supervisor, **Biology, METU** _____

Dr. Deniz Cansen Kahraman
Co-Supervisor, **Health Informatics, METU** _____

Examining Committee Members:

Prof. Dr. Sultan Baytaş
Pharmaceutical Chemistry, Gazi University _____

Prof. Dr. Mesut Muyan
Biology, Middle East Technical University _____

Assist. Prof. Dr. Aybar Can Acar
Health Informatics, Middle East Technical University _____

Date: 08.09.2021

I hereby declare that all information in this document has been obtained and presented in accordance with academic rules and ethical conduct. I also declare that, as required by these rules and conduct, I have fully cited and referenced all material and results that are not original to this work.

Name Last name : Büşra Bınarcı

Signature :

ABSTRACT

BIOACTIVITY ANALYSIS OF NOVEL INDOLE DERIVATIVES ON HEPATOCELLULAR CARCINOMA AS SIRTUIN INHIBITORS

Bınarcı, Büşra
Master of Science, Molecular Biology and Genetics
Supervisor : Prof. Dr. Mesut Muyan
Co-Supervisor: Dr. Deniz Cansen Kahraman

September 2021, 96 pages

Hepatocellular carcinoma is ruthless cancer, a subtype of primary liver cancer and affects many people with various ethnic backgrounds and age intervals. Indole derivative molecules are potent chemicals used in several drugs and target many essential proteins malfunctioning multiple diseases. One of the targets of indole derivatives is histone deacetylases (HDACs), which reverses histone acetylation modifications that open DNA to lead transcription machinery to promote transcription. This study screened 28 novel indole derivatives for their cytotoxicity capacity against three different cancer types. Four of them were selected based on the inhibitory concentration 50 (IC_{50}) values and structure-activity relations. Then, their targets were investigated with the DEEPScreen database and with molecular docking studies. In silico studies predicted that the molecules might interact with Sirt1, which is class III HDAC. For in vitro validation, the nuclear fraction of HCC cells was used in Sirtuin enzymatic activity assays. After the validation, one of the most critical targets of Sirt1, p53, which is also a vital tumor suppressor and mutagenized in HCC, was investigated. As a possible mechanism of action of the compounds, they could increase the acetyl-p53 level by blocking Sirt1 and lead p53-derived G1-mediated apoptosis in HCC cells.

Keywords: Sirtuin family, HCC, indole derivatives, anticancer activity

ÖZ

İNDOL TÜREVİ YENİ SİRTUIN İNHİBİTÖRLERİNİN HEPATOSELLÜLAR KARSİNOMA ÜZERİNDE BİYOAKTİVİTE ANALİZİ

Bınarcı, Büşra
Yüksek Lisans, Moleküler Biyoloji ve Genetik
Tez Yöneticisi: Prof. Dr. Mesut Muyan
Ortak Tez Yöneticisi: Dr. Deniz Cansen Kahraman

Eylül 2021, 96 sayfa

Primer karaciğer kanserinin alt sınıflarından olan hepatosellüler karsinoma (HSK) farklı etnik grup ve yaş aralıklarını etkileyen agresif bir kanser türüdür. Birçok ilacın yapıtaşlarından olan indol türevi moleküller hastalıkların oluşmasında rol alan birçok proteini hedefleyebilir. İndol türevi moleküllerin hedefleri arasında histon deasetilazlar (HDAC) da yer almaktadır. Bu enzim histon deasetilasyonunu sağlayarak DNA molekülünün transkripsiyon mekanizmasına bağlanmasını ve aktif hale gelmesini önler. Bu çalışmada, 28 yeni üretilen indol türevi moleküllerin 3 farklı kanser türüne karşı sitotoksisitesi araştırılmış ve en etkili olanları seçilmiştir. Seçilen moleküllerin olası hedef proteinleri DEEPScreen ve moleküler kenetlenme çalışmaları ile araştırılmış ve 3. Sınıf HDAC enzimi olan Sirt1 proteininin olabileceği saptanmıştır. *In silico* çalışmaların desteklenmesi için HSK hücrelerinin çekirdek kısmında enzimatik aktivite deneyleri yapılmıştır. Ayrıca, Sirt1'in hedeflediği, aynı zamanda HSK'de mutasyona uğramış önemli tümör baskılayıcı protein p53 de çalışılmıştır. Çalışma sonunda, moleküllerin muhtemel çalışma prensibi olarak Sirt1 enzimini bloklayıp p53 proteini aktif hale getirip HSK hücrelerinde G1 fazında tutuklama yaratıp hücrelerin apoptozuna sebep olabileceği saptanmıştır.

Anahtar Kelimeler: Sirtuin protein sınıfı, HSK, indol türevleri, antikanser aktivite

To my lovely family and my dear brother…

ACKNOWLEDGMENTS

Firstly, I would like to send my gratefulness to Chicago, our principal investigator of KanSiL lab, Prof. Dr. Rengül Çetin-Atalay. I appreciate her trust and belief in me even when I was an inexperienced 3rd-year undergraduate student. Her faith, with her acceptance of me to the lab, has changed my academic career forever.

Moreover, my co-advisor and my most significant educational trainer in this KanSiL journey, Dr. Deniz Cansen Kahraman, I am very thankful to you in my heart that none of the words can express my gratefulness to you. Lastly, my precious advisor, Professor Mesut Muyan, I appreciate your academic support and sharing your experiences to show me difficulties in academic life. You always solve my never-ending problems related to this thesis and academic career; thank you so much. In different words, also with my respect, this thesis would be meaningless without the supports of Dr. Deniz Cansen Kahraman and Prof. Mesut Muyan.

Dear Professor Sultan Baytaş from Gazi University and dear Assoc. Professor Tunca Doğan from Hacettepe University, thank you for supporting me in chemical structures and structural bioinformatics studies on the compounds.

I also wish to thank my KanSiL lab friends Altay Koyaş, Ece Kalem, Etkin Akar, Esra Nalbat, and Tuğçe Okşaklı. You were always there to support me with my academic problems and complete me for my insufficiencies on the field. Additionally, my friends and lovely colleagues from the Biology department, Sena Ezgin, Esra Çiçek, Emre Mert İpekoğlu, Burcu Tamkoç and Deniz Ak, your friendship and support were meaningful for me during this challenging journey. Also, professors from the department, Assist. Prof. Seçkin Eroğlu and Dr. İhsan Cihan Ayanoğlu, I am grateful that you are always there when I struggle with academic challenges.

Last but not least, I have to express my gratefulness for my lovely family. My mother, Süheyla and my father Bayram, and my brother, my best friend Burak, were always with me during this challenging journey. Without your emotional

support and faith in me, I couldn’t survive in this academia and create this work. Lastly, the cutest thing on Earth, our little rabbit, Tipsiz, I love you and thank you for your cuteness and fluffiness; without exaggeration, they are a huge motivation of my whole life!

This study was supported by the Ministry of Development, CansyL Project (Grant id: 2016K121540). Throughout this thesis period, I was supported by the TUBITAK-BIDEB 2210A National Master Candidate’s Scholarship program.

TABLE OF CONTENTS

LIST OF TABLES

LIST OF FIGURES

LIST OF ABBREVIATIONS

ADP	adenosine diphosphate
AMP	adenosine monophosphate
AMPK	AMP-activated protein kinase
BCA	bicinchoninic acid assay
BSA	bovine serum albumin
CI	cell index
CROssBAR	Comprehensive Resource of Biomedical Relations
CTNNB1	Catenin Beta 1
ddH_2O	double-distilled water
dH_2O	distilled water
DMEM	Dulbecco's Modified Eagle's medium
DMSO	Dimetyl Sulfoxide
DNA	deoxyribonucleic acid
DTT	Dithiothreitol
ECL	enhanced chemiluminescence
EGF/EGFR	epidermal growth factor/ epidermal growth factor receptor
EMT	epithelial to mesencymal transition
EtOH	ethanol
FBS	fetal bovine serum

FDA	food and drug administration
FGF/FGFR	fibroblast growth factor/ FGF receptor
FOXO	forkhead box O
HAT	histone acetyltransferase
HBV	Hepatitis B Virus
HCC	Hepatocellular Carcinoma
HCV	Hepatitis C Virus
HDAC	histone deacetylase
HGF	hepatocyte growth factor
HIF1α	hypoxia-induced factor alpha
HRP	horse reddish peroxidase
IC	inhibitory concentration
IGF/IGFR	insulin-like growth factor/ IGF receptor
lncRNA	long non-coding RNA
MAPK	mitogen-activated protein kinase
MetOH	methanol
mTOR	mammalian target of rapamycin
NAD	nicotinamide adenine dinucleotide
NAFLD	non-alcoholic fatty liver disease
ncRNA	non-coding RNA
NF-κB	Nuclear factor κB
NP-40	nonidet P-40

OD	optical density
PARP	poly ADP-ribose polymerase
PBS	phosphate-buffered saline
PDB	Protein Data Bank
PDGF/PDGFR	platelet-derived growth factor/ PDGF receptor
PGC-1α coactivator	peroxisome proliferator-activated receptor ϒ
PI	propidium iodide
Rb	retinoblastoma protein
RNA	ribonucleic acid
ROS	reactive oxygen species
RPMI	Roswell Park Memorial Institute
RT	room temperature
RTCEs	real-time cell electronic sensing system
SAR	structure-activity relationship
SDS	sodium dodecyl sulfate
Sir2	silent information regulator 2
Sirt	Sir2-like
SRB	sulforhodamine B assay
TBS	tris buffered saline
TBS	tris-base
TBS-T	tris buffered saline with Tween 20

TCA	trichloroacetic acid
TERT	telomerase reverse transcriptase
TNFα	tumor necrosis factor alpha
TP53	Tumor Protein 53
VEGF/VEGFR	vascular endothelial growth factor/VEGF receptor
WNT	Wingless and Int-1

CHAPTER 1

INTRODUCTION

Due to high incidence and mortality rates, a lot of people around the world suffer from cancer. Hepatocellular carcinoma is also a ruthless cancer type that affects many ethnic groups and age intervals. Apart from the mutagens, several metabolic diseases such as NAFLD, cirrhosis and viral infections result in HCC, which puts the illness at the center of many types of research. Targeted therapy is one of the most powerful methods to survive cancer. Since proteins are functional elements in a cell for various crucial processes such as proliferation, survival, immunity, etc., protein malfunctioning is the initial step to cancer in many cases. That is why targeting a compromised protein to fix it or block it can be an opportunity to kill cancer cells.

This thesis studied bioactivities and the effects of novel indole derivatives on hepatocellular carcinoma. For this purpose, newly synthesized indole derivative small molecules were investigated for their cytotoxicity against hepatocellular carcinoma cell lines. Indole derivatives are potent and promising candidates against cancer with less toxic effects on patients. Previous studies show that these compounds primarily target tyrosine kinases, estrogen receptors, topoisomerases, NFκB/PI_3/Akt/mTOR pathway, and HDACs. In addition, they also induce apoptosis, regulate tubulin assembly to interfere with tumorigenesis (Devi et al., 2021).

Firstly all compounds were screened against Huh7, MCF7, HCT116 cancer cell lines, and the most powerful ones were selected based on their cytotoxicity and structure for future studies. The IC_{50} concentrations and cytotoxicity of the molecules were determined with SRB assay. Since these molecules were novel and their targets were unknown, *in silico* screening for drug-target interaction estimation with the

selected molecules was performed with the DEEPScreen prediction algorithm. Sirtuin proteins were promising with a high probability for interactions. The findings were further investigated via AutoDock4 molecular docking software to estimate the target of the molecules. The most promising result was Sirt1 protein according to DEEPScreen and molecular docking studies.

Further validation of the *in silico* effects in vitro with Sirtuin enzymatic activity assay allowed us to hypothesize that these molecules might target Sirt1 to inhibit its function. Sirt1 is a class III HDAC, one of the favorite targets of indole derivatives, and it is overexpressed in HCC patients, which were the main factors that strengthened this hypothesis. Also, one of the targets of Sirt1, tumor suppressor protein p53, was investigated. Sirt1 deacetylases p53 to inhibit its function as tumor suppression in cancer cells. Blocking Sirt1 could elevate acetyl p53 level, which was investigated via western blot experiments in this study.

Furthermore, with IC_{100} concentrations, the real-time proliferation profile of HCC cells was monitored with the RTCEs system. Cell death (specifically apoptosis) mechanisms were studied with fluorometric methods, including Annexin V staining on flow cytometry and Hoechst staining on the fluorescent microscope and in protein level via Western Blot experiments. Lastly, cell cycle arrest was investigated via propidium iodide staining on flow cytometry.

CHAPTER 2

LITERATURE REVIEW

2.1 HEPATOCELLULAR CARCINOMA

Hepatocellular carcinoma (HCC) is the fourth most common reason for cancer-related deaths worldwide (*Cancer Today*, 2018.)**.** The epidemiology, risk factors, trends, molecular and phenotypic profiles of HCC have been resolved over the past few decades. Unfortunately, although valuable progress in understanding HCC has been made, the incidence and mortality continue to increase (Yang et al., 2019)**.**

2.1.1 Epidemiology

HCC is a subgroup of primary liver cancer, and it accounts for more than 80% of total primary liver cancer cases worldwide (Yang et al., 2019)**.** The incidence and mortality rates show variations in countries due to differences in demographic features, exposure to risk factors, and healthcare sources of countries (Mcglynn et al., 2015)**.** The age of onset of HCC also varies over countries (J. W. Park et al., 2015).

The survival rate of HCC varies over countries like other rates. One common aspect of this disease is that the survival rate dramatically decreases when time passes after the diagnosis. (Sarveazad et al., 2019).

2.1.2 Risk Factors

HCC develops when patients have chronic hepatitis B (HBV) and C (HCV) viruses, alcohol abuse, metabolic liver diseases (NAFLD, cirrhosis, obesity), exposure to toxins such as aflatoxins, aristolochic acid. Thus, each risk factor contributes differently to the initiation and progression of HCC in patients (Yang et al., 2019).

2.1.3 Pathogenesis of HCC

HCC pathogenesis involves several alterations affecting different molecular pathways and cellular events (Ho et al., 2016). However, thanks to both bioinformatic and wet-lab studies, the HCC metabolism and microenvironment have been resolving.

2.1.3.1 Genomic Alterations

Copy number alterations are observed in the HCC genome as gains and losses at several chromosomes according to whole genome and whole exome sequencing of HCC samples (Kan et al., 2013) (Schulze et al., 2015) (Totoki et al., 2014). 27-40% of HCC patients have a mutation in the β-catenin gene, a proto-oncogene in WNT signaling; it is also a putative driver for alcohol-related HCC (Ally et al., 2017). In addition, 21-31% of HCC patients have a mutation in TP53 protein, a master cell cycle regulator and a vital tumor suppressor protein (Ally et al., 2017). Another genetic alteration observed around 60% of HCC patients are recurrent somatic mutations in the promoter of TERT (Nault et al., 2013). This mutation is mainly detected during the transformation of premalignant lesions formed in cirrhosis into HCC (Nault et al., 2013). Among the risk factors of HCC, HBV is the one that directly integrates its viral genome into the human genome and disrupts

tumor suppressors or enhances proto-oncogenes and accounts for nearly 50% of HCC cases worldwide (El-Serag, 2011) (Lau et al., 2014).

2.1.3.2 Epigenetic Alterations

Misregulation of epigenetic mechanisms participates in HCC tumorigenesis. Several non-coding RNAs, microRNAs, piRNAs have been identified in HCC patients (Ma et al., 2014).

2.1.3.3 Altered Cell Signaling Pathways

Several cell signaling pathways have roles in HCC tumorigenesis, survival and metastasis with their downstream and upstream effects inside the cell. In brief, Wnt and Hedgehog signaling in differentiation and development, p53/p21 and RB1 signaling in genomic stability and cell cycle regulation, EGF/EGFR, HGF/MET, IGF/IGFR, PI3K/AKT/mTOR and RAS/MAPK growth factor-related signaling in cell survival, VEGF/VEGFR, PDGF/PDGFR and FGF/FGFR pathways in angiogenesis, JAK/STAT signaling in cytokine production are very crucial pathways that influence biological processes in HCC (Moeini et al., 2012) (Whittaker et al., 2010) (X. Wu & Li, 2012)(Figure 2.1).

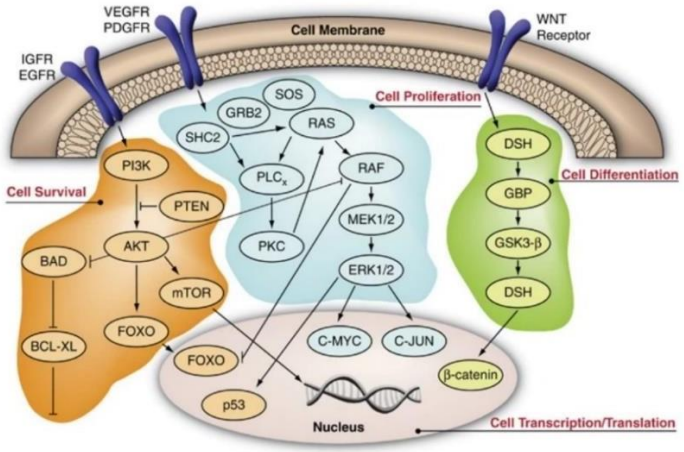

Figure 2.1: Schematic overview of signaling. Several cell signaling pathways with their essential roles in HCC cancer cells are seen. (License number: 5125921445891)

2.1.4 Prevention and Treatment of HCC

For the prevention of HCC, the elimination of risk factors are essential. For HBV and HCV infections, HBV vaccines are available. (Chang et al., 2016). Apart from chronic hepatitis, metabolic disorders are also risk factors for HCC. Pursuing a healthy lifestyle is a powerful strategy to keep the body healthy and free of metabolic disorders. Avoiding excessive alcohol, fast food consumption and smoking, minimizing dietary aflatoxin exposure, and spending time in exercising are very efficient ways to prevent liver injury due to fatty liver, leading to HCC (Patel et al., 2017) (Liu et al., 2012).

If HCC is not prevented, several treatment methods are followed, including surgical resection, liver transplantation, local ablation of tumor tissue, transarterial embolization, and radiotherapy (Yang et al., 2019). Additionally, there are systemic pharmacological treatment protocols available for the treatment of advanced-stage HCC patients. Sorafenib (small-molecule multikinase inhibitor), lenvatinib (multikinase inhibitor), cabozantinib (tyrosine kinase inhibitor), ramucirumab

(antiangiogenic) and nivolumab (immune checkpoint inhibitor) are some of the successful drugs that improve the survival of HCC patients (Yang et al., 2019).

2.2 EPIGENETICS

DNA is not kept in its linear state; instead, it is compacted into chromatin structures with nucleosomes formed from histones (Chen et al., 2014). Because of the compactness, transcription machinery cannot find a place to bind to DNA. Therefore, chromatin packages should be regulated to regulate gene transcription. This regulation is performed by epigenetic mechanisms that are inheritable gene expression changes without altering the DNA sequences (Chen et al., 2014).

2.2.1 Epigenetic Modifications

To coordinate gene expression, chromatin structure is remodeled with epigenetic modifications: DNA methylation, histone covalent modifications, and ncRNAs. These modifications build epigenetic codes modulating gene expression unique to cell types, differentiation stages and diseases (Sharma et al., 2009). In the scope of this study, only histone modifications, specifically histone acetylations, will be emphasized.

2.2.1.1 Histone Modifications

N-terminals of histones extend out of the nucleosome core, and the amino acids of the terminals can easily undergo covalent modifications: methylation, acetylation, sumoylation, ubiquitination, and phosphorylation (Bannister & Kouzarides, 2011). Individually or in combination, these covalent modifications regulate gene expression. The modifications are performed via enzymes. For histone acetylation, histone acetylases are utilized, which use acetyl-CoA as a cofactor and transfer the acetyl group to lysine amino acids on histone N-terminal tails for

acetylation. With acetylation, initially positively charged lysine groups are neutralized and even become negative. Since DNA is also negatively charged, acetylation event weakens the interactions between DNA and histones, making DNA more prone and available to let transcription factor binding and gene expression (Bannister & Kouzarides, 2011). HDACs, reverse this action and lead DNA to be more compact to interfere with gene expression. HDACs are composed of 4 different classes, and class III HDACs (Sirtuins) is the main topic within the context of this study.

2.3 SIRTUINS

Sirtuins are homolog of yeast Silent Information Regulators II (Sir2), and they use NAD^+ as a cofactor for deacetylation events. Humans have seven isoforms of sirtuins (Sirt1 to Sirt7) with different functions and various cell locations. Because of their connection to cancer, sirtuins are valuable therapeutic targets for cancer treatment strategies (Y. Wang et al., 2019).

2.3.1 Functions and localization of Sirtuin isoforms in human

Sirt1, Sirt6, Sirt7 mainly locate in the nucleus; Sirt3, Sirt4, Sirt5 are found in mitochondria, and Sirt2 is primarily in the cytoplasm. However, these locations can be tissue or cell type-specific and vary from cell to cell (Tanno et al., 2007). Although their localization differs, all Sirtuins share a common NAD^+ binding catalytic domain where deacetylation events occur. Via the catalytic domain, acetyl groups of proteins are transferred to ADP-ribose, and the deacetylated product is released (Liou et al., 2005) (Figure 2.3.1).

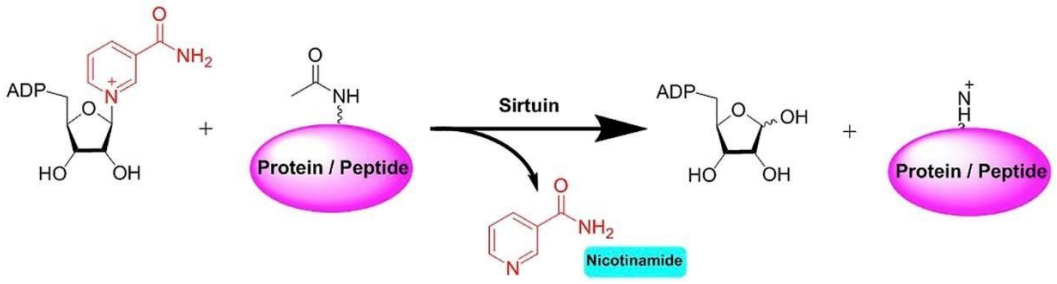

Figure 2.3.1: Schematic representation of deacetylation function of Sirtuins.

2.3.2 Sirtuin isoforms and diseases

Over the past few years, many studies reported that Sirtuin activity regulates various biological activities related to disease and the health status of life. Most importantly, several Sirtuin isoforms have roles in cancer and can be used as potential therapeutic targets for cancer treatment.

2.3.2.1 Sirt1

Sirt1 is the most well-studied member of the Sirtuin family in the nucleus and mainly involves mechanisms and diseases such as stress response, apoptosis, gene stability, cancer, and cardiovascular diseases by regulating acetylation status of NF-κB, FOXO1, HIF1α, p53 and Ku70 (Y. Wang et al., 2019). Sirt1 deacetylation prevents the tumor suppressor role of p53, which suppresses apoptosis in cancer cells and for this reason, some Sirt1 inhibitors are used to activate p53 function for anticancer activity (Heltweg et al., 2006). Likewise, Sirt1 deacetylation blocks FOXO protein family transcription, thereby FOXO-dependent apoptosis pathways in cancer cells (Brunet et al., 2004). Ku70 is also an essential protein that functions in DNA repair, and differently, Sirt1 deacetylation enhances Ku70 DNA repair

activity and participation in Bax-mediated apoptosis (Jeong et al., 2007). Deacetylation of NF-κB by Sirt1 sensitize cells to TNFα-induced apoptosis (Yeung et al., 2004). This paradox is always with Sirtuins; while they can be pro-apoptotic, they can be anti-apoptotic simultaneously. Likewise, while promoting cancer by blocking p53 tumor suppressor activity, they can prevent cancer by developing genome stability with Ku70 deacetylation.

2.3.2.2 Sirt2

Sirt2 localizes in the cytoplasm, and its main target is α-tubulin. α-tubulin deacetylation plays a role in the differentiation of oligodendrocytes, mainly found in glial cells in the central nervous system; that is why Sirt2 is primarily related to neurodegenerative disorders (Sakai et al., 2015). Also, Sirt2 deacetylases H4K16 histone, which regulates the cell cycle's G2 to M phase transition. Therefore, if Sirt2 is overexpressed in a cell, it delays the exit of cell division (Vaquero et al., 2006).

2.3.2.3 Sirt3

Sirt3 locates typically in the nucleus; however, when cells are under stress, Sirt3 goes to mitochondria to take action (Osborne et al., 2014). Thus, Sirt3 has a role in extending cell life by regulating cellular energy metabolism and removing ROS in mitochondria (Someya et al., 2010). Additionally, Sirt3 is found to be downregulated in many cancers such as breast, prostate, and hepatocellular carcinoma, suggesting that activation of Sirt3 may have anticancer effects for those cancers (Kim et al., 2010).

Unlike Sirt1-2-3, Sirt4-5-6-7 has less deacetylation function, and their mechanisms are still under investigation.

2.4 SIRT1 AND HEPATOCELLULAR CARCINOMA

One class III HDAC (Sirtuin) family member is Sirt1, which is overexpressed in HCC patients and cell lines (Al-Bahrani et al., 2015). Sirt1 overexpression can influence the activity of tumor suppressors and oncogenes that directly affect HCC progression.

2.4.1 Sirt1 overexpression promotes HCC metastasis

Sirt1 deacetylation function regulates EMT-related genes such as Snail and Twist (Palmirotta et al., 2016). Sirt1 deacetylation directly increases the activity of those EMT genes, promoting metastasis and invasiveness of HCC (Hao et al., 2014). Additionally, Sirt1 regulates HCC metastasis via PGC-1α protein. PGC-1α is a transcriptional coactivator that has a role in mitochondrial biogenesis and respiration. Also, PGC-1α is the direct target of Sirt1, and PGC-1α activation by Sirt1 promotes mitochondria biogenesis which alters energy metabolism and metastasis capacity of HCC (Li et al., 2016).

2.4.2 Sirt1 overexpression decreases survival of HCC

Patients who have a higher Sirt1 level have less chance of survival from HCC. Sirt1 level is also related to tumor size, and in advanced HCC, Sirt1 level is higher. However, there is a controversial situation for Sirt1 and HCC; in a healthy state, Sirt1 expression protects the body from malignancies. Therefore, it suggests that Sirt1 is beneficial for a healthy state and does not initiate HCC; however, when the tumor starts, Sirt1 changes its role (Farcas et al., 2019).

2.4.3 Sirt1 in cell growth and proliferation of HCC cell lines

When Sirt1 is silenced, inhibition of HCC cell line growth and cell cycle arrest (at G1 phase) is observed in one study (Choi et al., 2011). The acetylation status of p53 tumor suppressor protein with the regulation of Sirt1 deacetylation activity is involved in the mechanism of HCC cell survival. Sirt1 deacetylates and inactivates the tumor suppressor function of p53 upon DNA damage (Figure 2.4.1). Another study found that AMPK is downregulated in HCC cells. If AMPK is induced, it inhibits the deacetylation activity of Sirt1, which in turn increases acetylated and active p53 compared to control groups. Therefore, HCC cell growth is arrested at the G1 phase triggering apoptosis (Lee et al., 2012). That is why p53, one of the main targets of Sirt1, is a critical mediator for poor HCC cell survival due to overexpressed Sirt1.

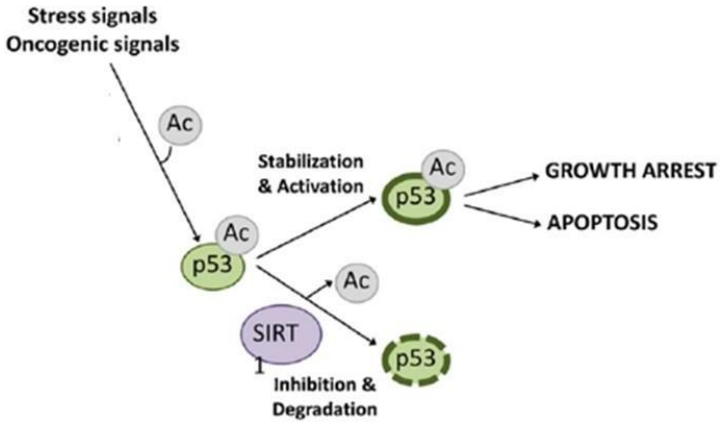

Figure 2.4.1: Sirt1 and p53 role in HCC proliferation. (License number: 5125930560322)

2.4.4 Sirt1 inhibition has an antitumor effect on HCC

Because of the tumor-promoting effects of Sirt1 expression in HCC, there are therapeutic approaches to inhibit Sirt1 from defeating HCC. Knockdown studies have shown that HCC proliferation regresses in vivo and in vitro (Portmann et al.,

2013). Sirtuin modulators mainly target Sirt1 since it is the most well-studied Sirtuin member, and also, Sirtuin families are conserved for their catalytic domains. To inhibit Sirt1 activity, many inhibitors are developed to defeat related diseases (Hu et al., 2014). Some Sirtuin inhibitors are listed below.

2.4.4.1 Dulcitol

Dulcitol is a natural product extracted from burning bush. Although its targets are still under investigation, in one study, dulcitol induces apoptosis by inhibiting Sirt1, which activates p53 tumor suppressor function in HepG2 cells (Lin et al., 2020) (Figure 1.4.2).

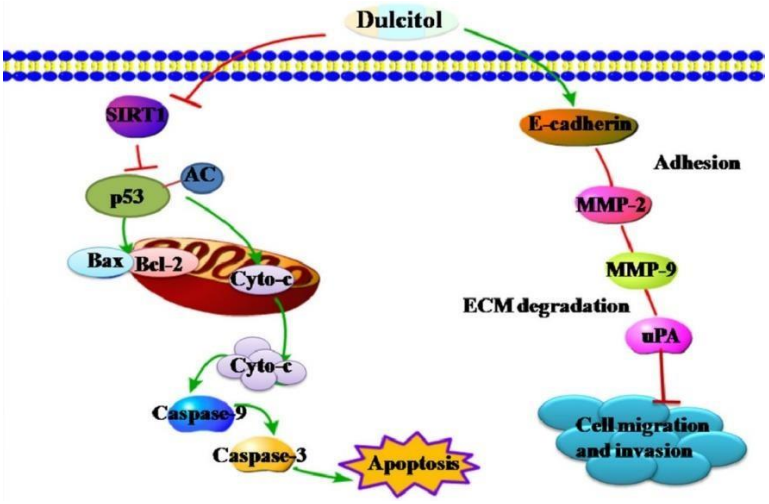

Figure 2.4.2: The mechanism of action of Dulcitol in HepG2 cells. (License number: 5125930768604)

2.4.4.2 Nicotinamide and its analogs

Nicotinamide is the first drug that is developed to target Sirtuins. It is effective on leukemia and prostate cancer (Audrito et al., 2011; Jung-Hynes et al.,

2009). Nicotinamides also inhibit HCC cell growth, induce apoptosis and increase acetyl p53 level in the early stage (S. Y. Park et al., 2012).

2.4.4.3 EX-527

This selective Sirt1 inhibitor is used as a drug for leukemia patients. For HCC, it is shown that EX-527 increases apoptosis and decreases cell migration and tumor growth both in vitro and in vivo (Farcas et al., 2019; Cea et al., 2011))

Many other Sirtuin inhibitors, such as Suramin, Tenovin and Splitomicin, are not effective against HCC, yet protective for other diseases (Hu et al., 2014).

2.5 Indole derivatives in cancer

Indole is a heterocyclic compound, and thanks to its versatile structure and relevance to many biologic elements, 80% of the therapeutic drugs contain this ring. Many antibiotics (penicillin, streptomycin, etc.), antidepressants (i.e., imipramine), diuretics (i.e., indapamide) and many more are heterocyclic moieties (Sachdeva et al., 2020).

Indole rings are counted as a “privileged scaffold” since they can bind to multiple receptors and proteins with high affinity. Therefore, they are preferable for researchers to design multi-target molecules for cancer therapy (Sravanthi & Manju, 2016). Indeed, nearly 60% of the anti-cancer compounds contain heterocyclic rings (Martins et al., 2015). Indoles can regulate DNA synthesis to control the proliferation and apoptosis of tumor cells (S. Wang et al., 2016). Additionally, indoles can influence the activity of the enzymes, which have a role in hepatitis viral replication, lipogenesis and metabolism of hepatotoxic substances to protect the liver, which is

essential to prevent HCC (S. Wang et al., 2016). Indole derivative compounds can also induce apoptosis and cell cycle arrest in HCC (Hawash et al., 2021).

2.6 Bioinformatics in cancer research

Bioinformatics is the utilization of informatics in biological studies such as cancer. With machine learning and artificial intelligence development, a natural system with its environment can easily be mimicked in a computer environment. Thanks to this improvement, invisible high-throughput data can be compared and contrasted with control groups or within groups with high accuracy and precision. The data could include drugs (drug banks), genes (gene banks), and proteins (proteomics) and reveal relations between them. De nova drug to protein interaction, stability, and affinity could be predicted and represented with an image via bioinformatics (D. Wu et al., 2012).

CanSyL (Cancer Systems Biology laboratory) develops powerful databases collaborating with various researchers and universities in Middle East Technical University. CROssBAR is a database that comprehensively integrates large-scale biological and clinical information to predict the connection between gene-protein, gene-gene, protein-protein, drug-protein, drug-drug, gene-drug (*CROssBAR Project*, n.d.). Additionally, DEEPScreen software, which is also utilized in this study, was developed by the same group to predict drug-to-target interactions (Rifaioglu et al., 2020).

CHAPTER 3

MATERIALS AND METHODS

3.1 MATERIALS

3.1.1 Cell Culture Reagents

All cell culture reagents, including the media, PBS, and the compounds for the treatment, were from different companies and are shown in Table 3.1.1.

Table 3.1.1: Cell Culture Reagents and equipment

Name	**Manufacturer**	**Catalog no**	**Storage**
Dulbecco's Modified Eagle's medium	Biological Industries	BI01-050-1A	+4 °C
Fetal bovine serum	Gibco™	10270	-20 °C
Non-essential amino acids	Lonza	BE12-114E	+4 °C
Penicillin/streptomycin	Gibco™	15140-122	-20 °C
RPMI 1640 medium	Biological Industries	BI01-104-1A	+4 °C
DMEM-F12	HyClone	SH30023.01	+4 °C
L-glutamine	Gibco™	25030	-20 °C
Phosphate-buffered saline	Gibco™	14190	RT

Trypsin-EDTA	Gibco™	25200	-20 °C
Dimethyl Sulfoxide (DMSO)	Sigma-Aldrich	D2650	RT
Selisistat (EX-527)	Selleckchem	S7577	+4 °C
Doxorobicine	DABUR	7AA015	+4 °C
Plates, cryovials	Corning Life Sciences (USA)		RT
Serological pipettes, sealed-cap polycarbonate centrifuge tubes	Costar Corporation (Cambridge)		RT

3.1.2 Reagents for Cytotoxicity Assay

The reagents required for the SRB assay and real-time RTCEs experiments are listed in Table 3.1.2.

Table 3.1.2: Reagents for SRB assay and RTCEs experiments

Name	**Manufacturer**	**Catalog No**	**Storage**
Trichloroacetic acid	Sigma-Aldrich	27242	+4 °C
Sulforhodamine B	Sigma-Aldrich	2S1403	RT
Tris-base	Sigma-Aldrich	T8524	+4 °C
E-plate 96	ACEA Biosciences	5232368001	RT

For the SRB assay, washing steps were performed with a Clonefill washing instrument (Genetix), and the absorbance values were read on the microplate reader (BMG Labtech, SuperStar Nano).

RTCEs plates were placed on its platform on a real-time cell analyzer instrument (ACEA Biosciences), and cell index values were obtained with the device.

3.1.3 Reagents for apoptosis detection and cell cycle analysis

Annexin V assay for apoptosis detection and propidium iodide staining for cell cycle profiling was performed via novocyte flow cytometer (ACEA Biosciences). Each experiment was performed with kits (Table 3.1.3).

Samples stained with Hoechst 33258 fluorescent dye were observed under the fluorescent microscope (Nikon elipse 5i with the ds-fi camera, Japan). The experiment's required equipment is seen in Table 3.1.3.

Table 3.1.3: Reagent required for apoptosis and cell cycle profiling studies.

Name	**Manufacturer**	**Catalog No**	**storage**
FITC Annexin V Apoptosis Detection	Parmingen, BD	556547	+4 °C
MUSE Cell Cycle Kit	Millipore	MCH100106	+4 °C
Hoechst 33258 dye	Sigma-Aldrich	33258	+4 °C
Coverslips	Marienfeld		RT

3.1.4 Reagents for western blotting

All the necessary solutions and materials for western blot experiments are shown in Table 3.1.4.

Table 3.1.4: Western blot reagents

Name	**Manufacturer**	**Catalog No**	
Mini PROTEAN TGX Stain-Free Gels	Bi-Rad	4568043-46	+4 °C
Odyssey Blocking buffer (PBS)	Li-cor	402-467-0973	+4 °C
Trans Blot Turbo 5X Transfer Buffer	Bio-Rad	10026938	+4 °C
Trans Blot LF PVDF Membrane and Filter Papers	BioRad	1620260	RT
Trans Blot PVDF Membrane	BioRad	1704156	RT
Bicinchoninic Acid Protein Assay Kit	Sigma	B9643	RT
Protease Inhibitor Cocktail Tablet	Roche	5892970001	+4 °C
PhosStop Tablet	Roche	4906837001	+4 °C
DTT	Carlo Erba	3086612	RT
Bradford Reagent	Sigma	B6B916	+4°C
Bovine Serum Albumin	Sigma	A7906	+4°C
SuperSignal WestFemto ECL	Thermo	34095	+4°C
Chameleon® Duo Pre-stained Protein Ladder	Li-cor	928-60000	-20°C
Chameleon® Vue Pre-stained Protein Ladder	Li-cor	928-50000	-20°C

Trans-Blot Turbo 5X Transfer Buffer	Bio-Rad	10026938	+4°C
10X Tris/Glycine/SDS (TGS) Running Buffer	Bio-Rad	161-0772	RT
Western Blot Running Tanks, transfer tools	Bio-Rad		RT

The power supply for the running of the gels was from Bio-Rad. In the chemiluminescent system, the images were taken with a C-Digit device (Li-cor). In the fluorescent method, the images were taken with an Odyssey-CLx device (Li-cor). The primary antibodies in the experiment are listed in Table 3.1.5, and the secondary antibodies are in Table 3.1.6.

Table 3.1.5: Primary antibodies that were used in western blot.

Antibody Name	**Manufacturer**	**Catalog No**	**Dilutions**
PARP	CST	9532S	1:500
p53	CST	9282S	1:1000
acetyl-p53 (Lys382)	CST	2525S	1:100
Sirt1	Santa Cruz	sc-15404	1:500
calnexin	CST	2679S	1:2000
B-actin	CST	4967	1:2000
HDAC1	Santa Cruz	sc- 81598	1:1000
GAPDH	ProteinTech	60004	1:10000

Table 3.1.6: Secondary antibodies that were used in western blot

Antibody	Manufacturer	Catalog no	Dilution	Method
Anti-rabbit	Sigma	A6154	1:5000	chemiluminescent
Anti-mouse	Sigma	T7782	1:5000	chemiluminescent
800CW anti-rabbit	Li-cor	32211	1:20000	fluorescent
680RD anti-rabbit	Li-cor	68071	1:20000	fluorescent

3.1.5 Reagents for the Sirtuin mechanism related experiments

For the Sirt1 ELISA experiment, SIRT1 Human SimpleStep ELISA Kit (ab171573) was used. For the enzymatic activity assay, Universal Sirt Activity Assay Kit (ab156915) was utilized.

3.1.6 General Reagents

Most of the chemicals and reagents used in the experiments are listed in Table 3.1.7.

Table 3.1.7: Chemicals used in the experiments

Name	Manufacturer	Catalog No	storage
Acetic Acid	Sigma	27725	RT
Ethanol	Sigma	E6133	RT
Methanol	Carlo Erba	41272	RT

Isopropanol	Sigma	34863	RT
Tween 20	Millipore	9005-64-5	RT
Sodium Dodecyl Sulfate	Bioshop	56-40-6	RT
Glycine	ACROS Organics	50-01-1	RT
Glycerole	Sigma	G9012	RT
NaCl	Applichem	A4555-0250	RT

3.2 SOLUTIONS AND MEDIA

3.2.1 Cell Culture Solutions

DMEM growth medium	10% Fetal Bovine Serum (FBS), 100 units/ml Penicillin/Streptomycin, 2 mM L-Glutamine, 1% non-essential aminoacids
RPMI 1640 growth medium	10% Fetal Bovine Serum (FBS), 100 units/ml Penicillin/Streptomycin, 2 mM L-Glutamine
DMEM- F12 growth medium	10% Fetal Bovine Serum (FBS), 100 units/ml

	Penicillin/Streptomycin, 2 mM L-Glutamine, 1% non-essential aminoacids, 20 ng/ml EGF, 10 ug/ul insulin, %2,5 Hydrocortisone
Freezing medium	10% DMSO in Fetal Bovine Serum (FBS)

3.2.2 SRB assay solutions

SRB stain	SRB stain was dissolved in 1% acetic acid as %0.4 w/v
%10 TCA	100% TCA was diluted with cold ddH_2O
10 mM Tris-Base (TBS)	Tris was dissolved in cold ddH_2O as %0,12 w/v

3.2.3 Western blotting and protein extraction solutions

1X PhosStop	1 tablet of Phosphatase Inhibitor tablet was dissolved in 1 ml ddH_2O

1X Protease Inhibitor Cocktail	1 tablet of protease inhibitor cocktail was dissolved in 1 ml ddH_2O
NP-40 lysis buffer	150 mM NaCl, 50 mM TrisHCl (pH=8), 1% NP-40, 0,1% SDS, 1X protease inhibitor cocktail, 1X phosphoStop in ddH_2O
10X Phosphate buffer saline (PBS)	80 gr NaCl, 2 gr KCl, 14.4 gr Na_2HPO_4, 2.4 gr KH_2PO_4 were dissolved in 1 ml ddH_2O; ph is adjusted to7.2 or 7.4
10X Tris buffered saline (TBS)	12.2% (w/v) of Trisma base, 87.8% (w/v) of NaCl in 1 ml ddH_2O, pH=7.6
TBS-T	0.1% Tween-20 was dissolved in 1X TBS
BSA Blocking buffer	5% (w/v) BSA in 0.1% TBS-T

1X Tris/glycine/SDS (TGS) running buffer	10X TGS was diluted with ddH_2O, the final volume was 600 ml per 2 gels.
Semi-dry transfer buffer (for 1 L)	200 ml 5X Trans-Blot Transfer Buffer, 200 ml EtOH, 600 ml cold ddH_2O
Mild stripping buffer (for 100 ml)	1.5 g Glycine, 0.1 g SDS, 1 ml Tween 20, 100 ml ddH_2O, adjusting ph to 2.2

3.3 METHODS

3.3.1 In silico studies

3.3.1.1 DEEPScreen Drug-Target Predictions

First, as a query, SMILES form of the compounds (Table 3.3.1) are submitted to DEEPScreen, which converts them to 2-D images and learns complex features from these representations with deep convolutional neural networks. Then the software facilitates these properties to discover unknown drug-target interactions (Rifaioglu et al., 2020). The information related to the proteins (targets) comes from the curated bioactivity data. The highly optimized software has a sophisticated algorithm to include positive, negative, and internal controls to provide the best predictions.

ChEMBL identity numbers given in Table 3.3.1 were used in the predictions.

Table 3.3.1: Identity of the inputs used in DEEPScreen

Target name	**ChEMBL Id***
Sirt1	CHEMBL4506
Sirt2	CHEMBL4462
Sirt3	CHEMBL4461
Compound name	**Canonical Smiles****
EK-79	Cn1c2ccccc2cc1c1nnc(n1Cc1ccccc1)SCc1ccc(cc1)C(F)(F)F
EK-99	Cn1c2ccccc2cc1c1nnc(n1Cc1ccccc1)SCc1ccc(cc1)OC(F)(F)F
EK-101	Cn1c2ccccc2cc1c1nnc(n1c1ccccc1)SCc1ccc(cc1)C(F)(F)F
EKK-115	Cn1c2ccccc2cc1c1nnc(n1CCc1ccccc1)SCc1ccc(cc1)C(F)(F)F

*Extracted from ChEMBL database (https://www.ebi.ac.uk/chembl/)

**Created with Open Babel GUI software

3.3.1.2 Molecular Docking Studies

For Sirt1 protein, PDB id= 4i5i; for Sirt2 protein, PDB id; 4rmg were used. From the 4i5i PDB file, the atomic coordinates of EX-527 were removed. From the 4rmg PDB file, SirReal2 atomic coordinates were erased. The atomic coordinates for NAD^+ were kept in both files. Then files were loaded to AutoDock4 software, and grid box centers were set to 12.336, -6.797, 23.362 for Sirt1 docking studies, and -13.855, -20.491, 0.664 for Sirt2 dockings. In all docking studies, grid points were 60,60,60 for x,y, and z, respectively. The spacing was 0.375 A°.

The 3D structure of the novel compounds was first created with ChemSketch software and converted to a PDB file via Open Babel GUI software.

3.3.2 Cell Culture and Treatment

HCT116, MCF7, Huh7, HepG2, Hep3B, Hep3B-TR, Mahlavu were maintained in DMEM. SNU475 was held in RPMI 1640; DMEM-F12 medium was used for MCF12A. All cells were incubated at 37°C in a humidified 5% CO2, 95% air incubator.

Indole derivative compounds for the screening were synthesized at Gazi University, Department of Pharmaceutical Chemistry (collaboration with Prof. Dr. Sultan Baytaş). The compounds were dissolved in DMSO as 40 mM stocks according to the formula below:

$$\mathbf{M} = \frac{\mathbf{n}}{\mathbf{v}} \qquad \mathbf{n} = \frac{\mathbf{m}}{\mathbf{M_w}}, \textbf{ so=> } \boldsymbol{M = \frac{\frac{m}{M_m}}{v}}$$

For the treatment, cells were seeded to the respective plates with optimized numbers (Table 3.3.2.1 and 3.3.2.2). After 24 hours from the seeding, media was removed, and cells were washed with 1X PBS. New media with the compounds was added to cells. Vehicle control/negative control cells were treated with only DMSO (final concentration does not exceed %0.2 v/v). Cells in the positive control group were treated with commercial SIRT1 inhibitor EX-527 or doxorubicin.

Table 3.3.2.1: Number of cells seeded to 96-well plates

Cell line	Number of cells per well (96-well plate)
Huh7	2000 cell/well
SNU475	2000 cell/well
Mahlavu	1000 cell/well
HepG2	3000 cell/well
Hep3B-TR	2000 cell/well
Mcf7	2000 cell/well
HCT116	3000 cell/well
MCF12A	7000 cell/well

Table 3.3.2.2: Number of Huh7 and SNU475 cells seeded to different plates

	12-well plate (cell/well)	6-well plate (cell/well)	100mm dish (cell/dish)	150mm dish (cell/dish)
Huh7	30.000	60.000	200.000	500.000
SNU475	20.000	40.000	150.000	375.000

3.3.3 General Cell Culture Techniques

3.3.3.1 Cell Freezing

The cells were precipitated via centrifuge, at 1800 rpm, for 5 minutes. Then, the supernatant was discarded, and the pellet was resuspended in a freezing medium (1 ml/10^6 cells). The suspensions were transferred to cryovials, which were stored at -80° then in liquid nitrogen.

3.3.3.2 Cell Thawing

The frozen cells were taken from liquid nitrogen and heated at 40° for 2-3 minutes in the water bath. Then the freezing medium was diluted via the respective medium of the cell of interest, and it was removed with centrifugation at 1500 rpm, for 5 minutes, at +4°. The next day, the cells were checked, and if they were confluent enough, they were passaged; if not, the medium was changed to remove dead and unattached cells from the environment.

3.3.3.3 Cell Passaging

When cells reached 80-90% of confluency within 3-4 days, a portion of the cells (1:20 to 1:5 depends on confluency) were passaged to new dishes for

continuous growth. First, the old medium was aspirated, and plates were washed with 1X PBS to remove all medium remainings. Then the adequate amount of trypsin to cover the surface of the dishes was added and incubated for 2-3 minutes at the incubator to detach cells. After that, the respective medium was added to stop trypsin activity, and cells were resuspended in their medium. According to passaging dilution, the corresponding portions of cells were seeded into new dishes.

3.3.4 NCI-60 SRB assay

Huh7, SNU475, Mahlavu, HepG2, Hep3B-TR, Mcf7, HCT116 and MCF12A cells were seeded in triplicates to 96-well plates (Table 3.3.2.1) in 150 µl media. After 24 hours, the medium was refreshed, and the compounds dissolved in DMSO were applied as 40 µM, 20 µM, 10 µM, 5 µM, and 2.5 µM concentrations. DMSO was also used with the same concentrations as vehicle control. After 72 hours of incubation with the compounds, the medium was removed, and wells were washed with 1X PBS. Then, cells were fixed with 50 µl of 10% TCA and kept at 4°C in the dark for 1 hour. TCA fixation was ended by washing wells with ddH_2O four times. Wells were stained with 50 µl of 0.4% SRB dissolved in 1% acetic acid solution for 15 minutes in the dark at room temperature. After the staining, wells were washed with 100 µl of 1% acetic acid. SRB dye was solubilized in 10 mM Tris-base (pH=8) for 15 minutes on the shaker at room temperature. Absorbance values were obtained at 515 nm with a microplate reader. Values were normalized against DMSO treated wells to detect the growth inhibition percentage of the compounds for each concentration, and IC_{50} concentrations were determined using the concentration versus percent inhibition curves generated.

3.3.5 Real-time Electronic Sensing (RTCEs) for Cytotoxicity testing

Huh7, HepG2, Mahlavu, SNU475 and Hep3B-TR cells were seeded in triplicates in 100 µl media (Table 3.3.2.1) to E-Plate 96 plates which were placed on

xCELLigence station in 5% CO2 at 37 °C incubators. The cell index (CI) values were recorded every 30 minutes. After 24 hours, the medium was refreshed with 100 µl of the medium containing IC_{50} and IC_{100} concentrations of the compounds and DMSO. CI values were recorded every 30 minutes for 72 hours to observe the real-time response of the cancer cells to the compounds.

3.3.6 Apoptosis Detection

3.3.6.1 Annexin V assay

When cells undergo apoptosis, phosphatidylserine residues flip to the extracellular environment from an intracellular place. Annexin V can stain these extracellular phosphatidylserine residues to measure apoptosis. Huh7 and SNU475 cells were seeded to 6-well plates(Table 3.3.2.2). After 24 hours, the old medium was refreshed with new media containing an IC_{100} concentration of the compounds. After 24 hours of treatments, all the attached and detached cells were collected and resuspended with Annexin V Apoptosis Detection kit's 1X assay buffer as 100 µl per 10^6 cells. Then kit's protocol was followed to detect early and late apoptotic cells on flow cytometry.

3.3.6.2 Immunohistochemistry Staining with Hoechst 33258 fluorescent dye

Huh7 and SNU475 cells seeded with coverslips (Table 3.3.2.2). The next day, the medium was refreshed, and the IC_{100} concentration of the compounds was given to cells on the coverslips. After 12,24,36,48, and 72 hours of treatment, the media were aspirated, wells were washed twice with 1X PBS, and cold 100% Methanol was added to the cells for fixation. Cells were fixed and permeabilized for 10 minutes. Then methanol was removed, and cells were washed with 1X PBS twice.

For the staining, Hoechst 33258 (300 µg/ml) was prepared as a 1 µg/ml stain (%v/v) in 1X PBS (400 µl/well). After 5 minutes of incubation with the dye at room temperature and at dark, ddH_2O was used for washing. Then for the destaining process, the wells were incubated with ddH_2O at dark, at room temperature for 10 minutes. Finally, coverslips were mounted on slides with a tiny drop of glycerol to visualize stained nuclei under the fluorescent microscope.

3.3.7 Cell Cycle Analysis with Propidium Iodide Staining

Huh7 and SNU475 cells were seeded to 6-well plates (Table 3.3.2.2). After 24 hours, the old media were refreshed with new media containing the IC_{100} concentration of the compounds. After 24 hours of the treatment, all the attached and detached cells were collected, and pellets were fixed with 1 ml cold 70% EtOH on the vortex. After at least 3 hours of fixation at -20°, EtOH was removed by diluting it with cold PBS and centrifugation at 2000 rpm, 5 minutes, +4°. Then, fixed cells were stained with the propidium iodide solution as 200 µl per 10^6 cells. The manufacturer's protocol was followed for the analysis (MUSE Cell Cycle Kit, Millipore, MCH100106).

3.3.8 Western Blotting

3.3.8.1 Sample Preparation

Huh7 and SNU475 cells were seeded to dishes (Table 3.3.2.1). The next day, the media were refreshed with the media containing IC_{100} concentration of the compounds 24 or 48 hours, depending on the proteins explored. The old media and collected cells (scraped in 1X PBS on ice) were precipitated via centrifugation with 13.000 rpm, 6 minutes and at +4°. The precipitated cells were washed with cold 1X PBS at 1800 rpm for 5 minutes centrifugation.

3.3.8.1.1 Crude Protein Extraction

The 1X PBS was aspirated, and according to the pellet volume, 20 to 100 µl NP-40 lysis buffer was used for resuspension. The pellets were incubated on ice for 45 minutes and every 10 minutes intervals; samples were on vortex to speed up the lysis process. Then the proteins were collected via centrifugation at 14.000 rpm for 20 minutes at +4°. Extracted proteins were in the supernatant.

3.3.8.1.2 Nuclear and Cytoplasmic Protein Extraction

Nuclear Extraction Kit (ab113474) protocol was followed to separate cytoplasmic proteins from nuclear proteins.

3.3.8.2 Protein Quantification

3.3.8.2.1 Bicinchoninic Acid (BCA) Assay

Bicinchoninic Acid Protein Assay Kit (B9643) was utilized to quantify proteins isolated via crude protein extraction. A 25 µl sample was mixed with a 200 µl BCA working reagent (containing a 1:50 ratio of volumes from reagent A and

reagent B, respectively). The standard proteins were prepared as 2mg/ml, 1mg/ml, 0.5mg/ml, 0.25mg/ml and 0.125mg/ml BSA protein (20mg/ml stock) by ddH_2O as diluent. ddH_2O was used as blank as well. When the samples, standards and blank conditions were added to 96-well microplate wells, the incubation with the working reagent was performed at 37°C, for 30 minutes. After incubation, the plate was read on 562 nm, blank absorbance value (OD) was subtracted from the sample and standard OD, the standard curve was created with the standard proteins. With linear regression, the equation was found (y=ax, a was the slope). Then OD

values of the samples were used (as y in the equation) to determine their concentration (x in the equation).

3.3.8.2.2 Bradford Assay

The concentration of the samples whose proteins were separated as nuclear and cytoplasmic ones were determined with Bradford assay as suggested by the Nuclear Extraction Kit's protocol. For the Bradford assay, 5 µl of the samples were mixed with 250 µl of Bradford reagent for the reaction. Standard proteins were prepared the same as the BCA assay. All conditions with Bradford reagent were added to 96-well microplates and incubated on the shaker, at dark, for 3 minutes at room temperature. Then the absorbance values were read on 495 nm, and the concentrations were calculated the same as in the BCA protocol.

3.3.8.3 Gel loading and Running

15 well or 10 well comb stain-free ready-to-use gels were used for Western Blot. For 15 wells comb gels, 20 µg to 50 µg proteins in 12 µl; for 10 well comb gels, 40 µg proteins in 25 µl were loaded. Before sample loading to the wells, the mix of the protein, DTT, loading dye was prepared and heated at 95°C for 7 minutes for denaturation of the proteins. Then samples were spun down. The Bio-Rad system was used for all Western Blot experiments.

Running was done for 30-40 minutes with 120V with TBS running buffer.

Two systems were utilized for western blot experiments, which are fluorescent systems and chemiluminescent systems. For both the methods, cassette preparations, gels, and running conditions were the same, but the ladder and loading buffers differed. An autofluorescent ladder that can also be visible (Chameleon Duo, Licor) was used in the fluorescent system. In the chemiluminescent system, a visible protein ladder (Chameleon Vue, Licor) was utilized.

3.3.8.4 Semi-dry transfer

In the fluorescent system, the low-fluorescent (LF) PVDF membrane; in the chemiluminescent system, the PVDF membrane was used.

For the semi-dry transfer, semi-dry transfer buffer and Trans-Blot transfer devices were utilized. First, the membranes were soaked in MetOH for 30 seconds to activate them. Next, the transfer stacks were soaked into transfer buffer for 2 minutes. The membrane and gel were placed between two transfer stacks, and the system was set to Trans-Blot.

3.3.8.5 Blocking

For the fluorescent system, LICOR's Oddesy Blocking buffer (PBS) to the membrane was added and incubated for an hour at room temperature or overnight at +4°C with gentle shaking.

The same protocol was applied with %5 BSA in %0.1 TBS-T blocking buffer to block the membrane in the chemiluminescent system.

3.3.8.6 Primary and secondary antibody incubations

For each system, the primary antibodies were prepared in their blocking buffers. Only in the fluorescent method, %0.01 (v/v) Tween20 was added as well. Primary antibody incubation was performed for 2 hours at room temperature or overnight at +4°C with gently shaking. When incubation was over, if the fluorescent system was utilized, three times washing (5 minutes per each) with %0.1 TBS-T; and if the chemiluminescent procedure was followed, five times washing (5 minutes X2, 10 minutes, 5 minutes X2) with %0.1 TBS-T with the agitation was done.

For the chemiluminescent system, HRP-conjugated anti-mouse or anti-rabbit secondary antibodies were used in its blocking buffer. Fluorescently conjugated anti-

rabbit or anti-mouse secondary antibodies were prepared in its blocking buffer with %0.1 Tween and %0.02 SDS in the fluorescent system. The incubation time for the secondary antibodies was an hour at room temperature with gentle shaking. Fluorescent antibodies were incubated in the dark. The washing steps were the same as the previous one.

3.3.8.7 Visualization of the membranes

In the chemiluminescent system, the membranes were incubated with ECL substrate (reagent A and reagent B as a 1:1 volume) in the dark for 5 minutes. After incubation, the membranes were visualized.

3.3.8.8 Stripping

In the chemiluminescent system, if necessary, the membranes were stripped for re-incubations. After the image was taken, ECL-substrate was removed by rinsing the membrane with ddH_2O. Then the membrane was stripped in mild stripping buffer for 15 minutes with agitation. Finally, the membrane was washed with %0.1 TBS-T for 5 minutes 3 times, and blocking was done before the primary antibody incubation.

3.3.9 Human Sirt1 ELISA

Samples were prepared by seeding Huh7 and SNU475 to dishes (Table 3.3.2.2). Since the basal level of Sirt1 was investigated, no treatment was done, and cells let to grow for 3-4 days. When cells reached confluency, they were scraped, and proteins were isolated with Nuclear Extraction Kit (ab113473). Sirt1 standard protein (200ng/ml stock) was prepared as 200ng/ml, 100ng/ml, 50ng/ml, 25ng/ml 12.5ng/ml, and 6.25ng/ml. SIRT1 Human SimpleStep ELISA Kit (ab171573)'s protocol was followed. ELISA plate was read at 450 nm. An S-shape standard curve

was constructed, and the basal amount of Sirt1 in Huh7 and SNU475 cells was calculated in the ng unit.

3.3.10 Enzymatic Activity Assay

Samples were prepared by seeding Huh7 and SNU475 to dishes (Table 3.3.2.2). Cells were grown for 2-3 days without treatment. Then, they were scraped, and proteins were isolated with Nuclear Extraction Kit (ab113473). Standards (deacetylated histones in 50ng/µl stock) were prepared as 80ng, 40ng, 20ng, 10ng, and 5 ng. Universal Sirt Activity Assay Kit (ab156915)'s protocol was followed, and the plate read at 450 nm and 655 nm.

Inhibition calculations;

Firstly OD values at 655 nm were subtracted from OD values at 450 nm.

Then this formula was followed;

$Inhibition\ \% = 1 - ((\ Inhibitor\ Sample\ OD - NNC\ OD)/(No\ Inhibitor\ Sample\ OD - NNC\ OD))\times 100\%$

NNC is the negative control that has no cofactor in it.

CHAPTER 4

RESULTS

There were 28 newly designed and synthesized compounds to study. Firstly, their general cytotoxicity against several cancer types was studied to select the most potent molecules, considering their structure-activity relationships. Secondly, with the selected molecules, their possible targets were predicted with *in silico* studies, and the predictions were validated with in vitro methods in HCC. Lastly, the most potent compounds' general cytotoxicity, their effect on HCC cell survival were investigated.

4.1 The selection of the most potent compounds

Although HCC cancer progression was the main focus, before going deep into HCC, all 28 compounds were screened against colon, breast and HCC representative cancer cell types to reveal their anti-cancer property. The cytotoxicity of the compounds against HCC, breast cancer and colon cancer cell lines were assessed with SRB assay, which is also used to calculate the IC_{50} concentrations of the molecules.

Calculated IC_{50} values of the compounds were below 10 μM concentration yet; some were not very effective with IC_{50} values reaching 30-40 μM and more (Table 4.1). Based on the IC_{50} values and structure-activity relationships, EK-79, EK-99, EK-101 (leading compound) and EKK-115 were selected for further experiments.

Table 4.1: IC_{50} (μM) values of novel indole derivatives on Huh7 (HCC); MCF7 (breast cancer); HCT116 (colon cancer) with NCI-60 SRB assay, after 72 hours

		IC_{50} (μM)*		
Compound	**Chemical Structure**	**Huh7**	**MCF7**	**HCT116**
EK-21	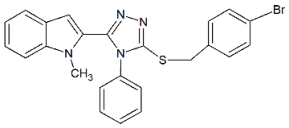	3.8	11.0	15.1
EK-23	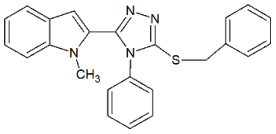	17.0	10.7	14.1
EK-31	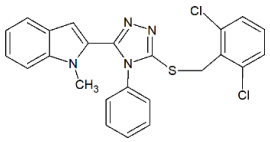	1.9	6.1	9.3
EK-33	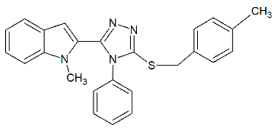	7.5	21.2	38.6
EK-41	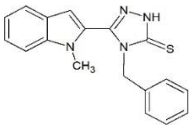	14.1	17.4	22.7
EK-43	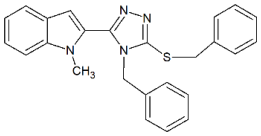	4.5	11.8	17.3
EK-45	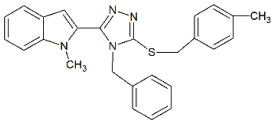	3.4	8.1	28.0

EK-47	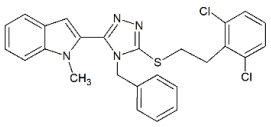	4.2	5.8	10.3
EK-49	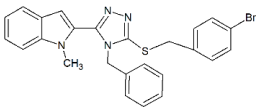	0.8	8.5	7.6
EK-75	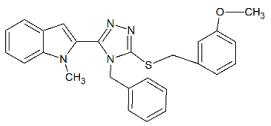	2.0	9.5	9.5
EK-77	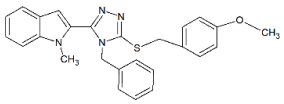	3.5	7.4	10.6
EK-79**	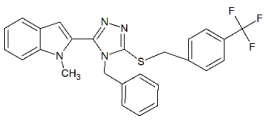	1.3	6.2	5.7
EK-81	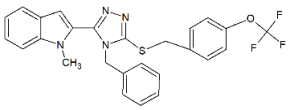	2.5	6.5	7.8
EK-83	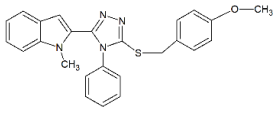	4.2	15.2	2.7
EK-95	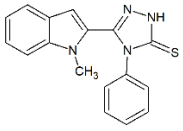	22.4	31.4	>40

EK-97	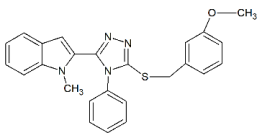	0.8	11.7	7.3
EK-99**	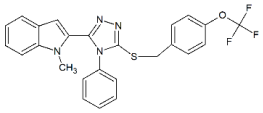	0.5	3.2	2.5
EK-101 **,***	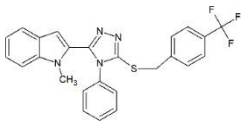	0.1	4.8	5.2
EKK-85	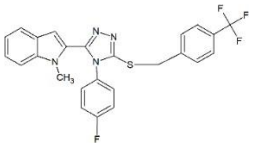	8.7	6.5	7.2
EKK-86	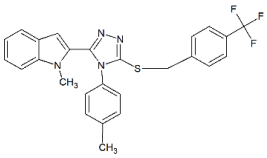	9.8	14.4	11.9
EKK-87	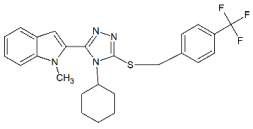	4.3	7.1	4.8
EKK-88	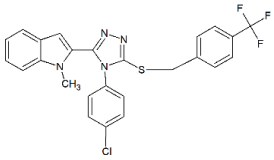	12.2	3.7	3.9
EKK-90	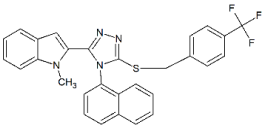	6.4	9.9	3.2

EKK-110	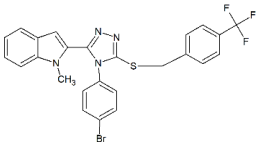	11.8	11.7	12.2
EKK-111	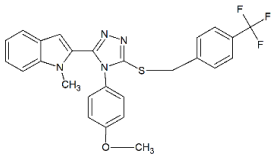	8.9	8.2	8.9
EKK-113	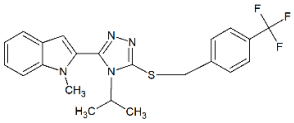	6.6	6.9	6.4
EKK-114	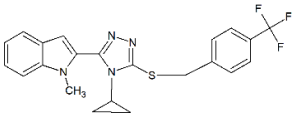	8.3	9.9	7.8
EKK-115**	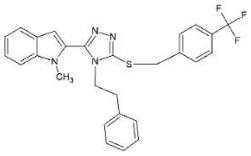	4.5	6.2	4.0

*R^2 values were within the range of 0.7 to 0.99, and standard deviations were less than ±10% for each value. The experiments were performed as triplicates.

**Selected compounds based on the IC_{50} values

***The lead compound from which all other structures were derived.

4.2 Target predictions for the compounds

After the selection, DEEPScreen software was used to predict drug-target interactions with high accuracy. Then, obtained targets were used in Autodock4 software to dock the potent compounds to the possible targets for further validation.

Lastly, one of the small molecule inhibitors, whose target was found in DEEPScreen results, was investigated for its similarity to the compounds.

4.2.1 DEEPScreen drug-target interaction predictions

The prediction study revealed that selected compounds might actively interact with Sirt1 and Sirt2 proteins from the Sirtuin family (Table 4.2.1).

The results have shown that EK-79, EK-99, EK-101, and EKK-115 are predicted to interact with Sirt1 and Sirt2 but not with Sirt3. Since the predictions' accuracy was very high (more than %50), further in silico and in vitro analysis of these compounds continued during the study (Table 4.2.1).

Table 4.2.1: The predictions from DEEPScreen analysis for the interactions between Sirt1, Sirt2, Sirt3 and the novel indole derivatives

Compound	Sirt1	Sirt2	Sirt3
EK-79	**Active**	**Active**	**Inactive**
EK-99	**Inactive**	**Active**	**Inactive**
EK-101	**Active**	**Active**	**Inactive**
EKK-115	**Active**	**Inactive**	**Inactive**
Accuracy (%)	**%75**	**%85**	**%80**

* Active: there is an active drug-target interaction

** Inactive: there is an inactive drug-target interaction (no interaction)

*** Accuracy: Performance of the prediction model, indicating the reliability of predictions.

4.2.2 Molecular Docking Studies with Autodock4

To further validate the DEEPScreen results, molecular docking studies have been performed between EK-79, EK-99, EK-101, EKK-115 molecules and Sirt1-Sirt2 proteins. For molecular docking, AutoDock4 software was utilized (Morris et al.,

2009). The estimated free energy for binding the compounds and Sirt1 was promising (Figure 4.1.2.1 and Table 4.1.2.1).

A. **Docking of EX-527 to Sirt1, ΔG= -9.82**

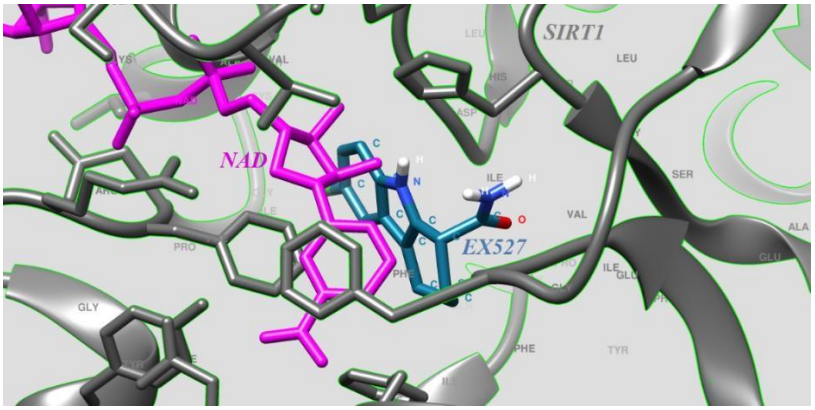

B. **Docking of EK-79 to Sirt1. ΔG= -11.44 kcal/mol**

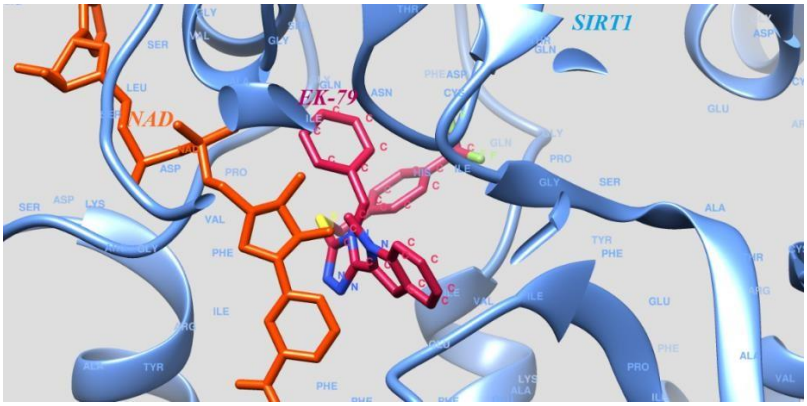

C. **Docking of EK-99 to Sirt1, ΔG= -7.12 kcal/mol**

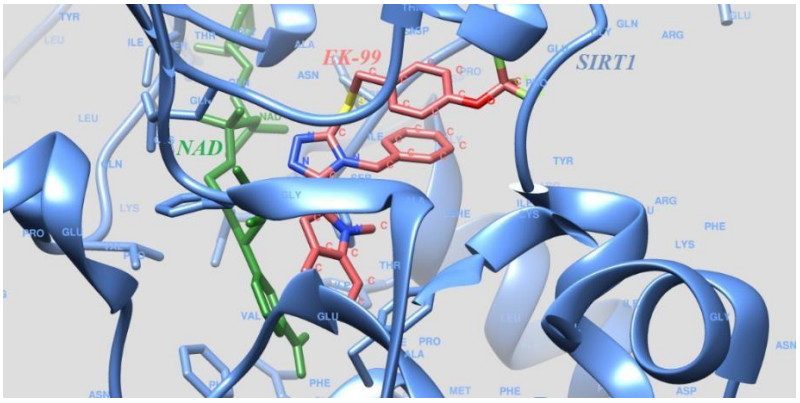

D. **Docking of EK-101 to Sirt1, ΔG= -11.32 kcal/mol**

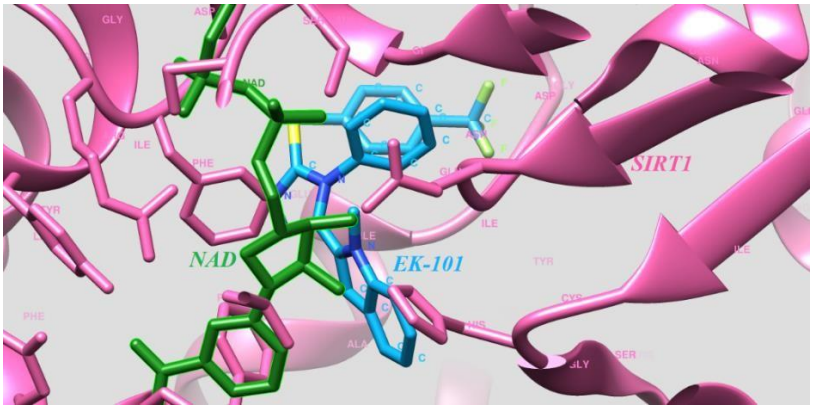

E. **Docking of EKK-115 to Sirt1, ΔG= -7.40 kcal/mol**

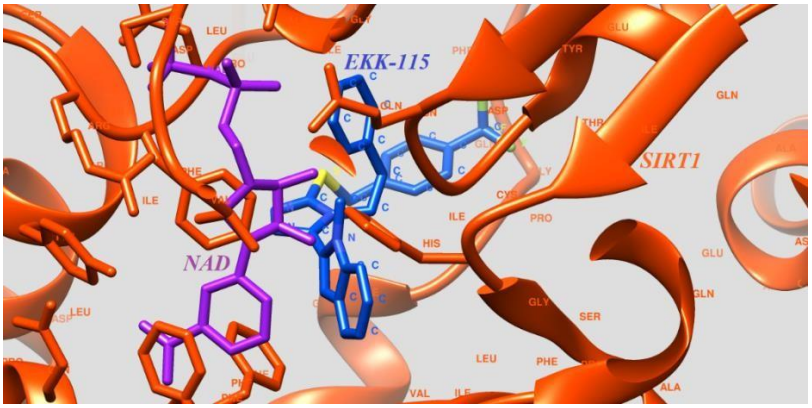

Figure 4.2.2.1: Visualization of molecular docking of the compounds to Sirt1. Docking of Sirt1 to **A.** EX-527 **B.** EK-79 **C.** EK-99 **D.** EK-101, and **E.** EKK-115 in the presence of NAD^+ cofactor. (Figures created in Chimera 1.15 RC)

The .dlg file retrieved from each molecular docking process in Autodock4 provides estimated binding energy (ΔG) for the best docking pose between the molecule and the target (Malmstrom & Watowich, 2011). The calculated binding energy for the best docking pose was less than -7 (Table 4.2.2.1) for all the compounds.

Table 4.2.2.1: Estimated binding free energy of the docking of the compounds to Sirt1

Compound	Binding free energy
EK-79	ΔG= -11.44 kcal/mol
EK-99	ΔG= -7.12 kcal/mol
EK-101	ΔG= -11.32 kcal/mol
EKK-115	ΔG= -7.40 kcal/mol
EX-527	ΔG= -9.82 kcal/mol

The EK-79, EK-99, EK-101, and EKK-115 docking to the Sirt2 part is seen in Figure 4.2.2.2.

A. **Docking of SiReal2 to Sirt2, ΔG= -7.12 kcal/mol**

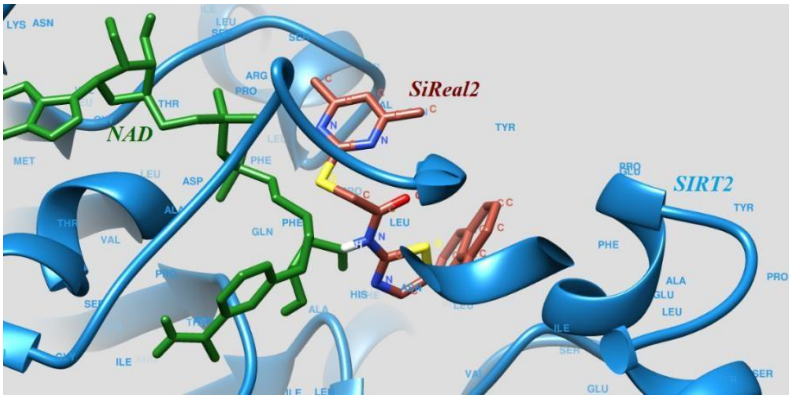

B. **Docking of EK-79 to Sirt2, ΔG= -7.75 kcal/mol**

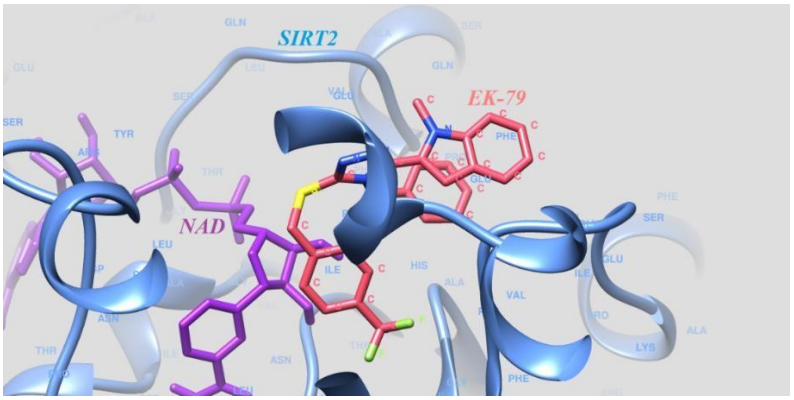

C. **Docking of EK-99 to Sirt2, ΔG= -6.80 kcal/mol**

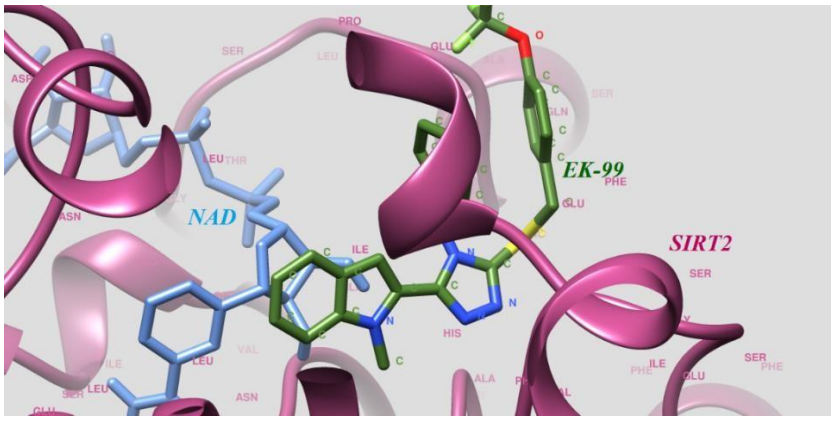

D. **Docking of EK-101 to Sirt2, ΔG= -7.78 kcal/mol**

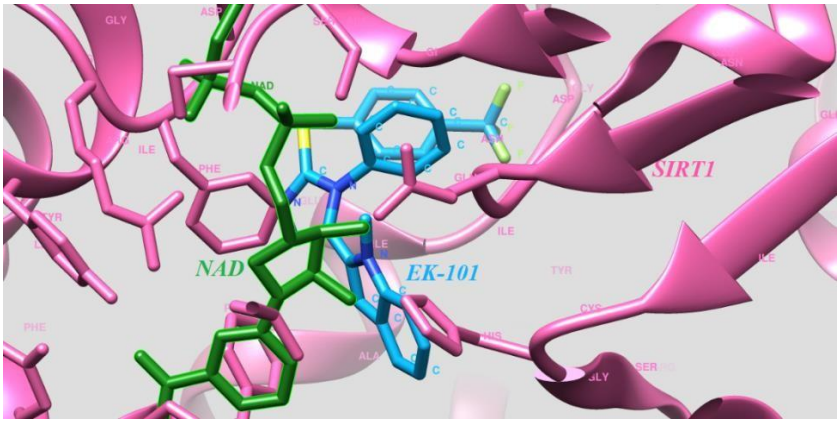

E. **Docking of EKK-115 to Sirt2, ΔG= -6.68 kcal/mol**

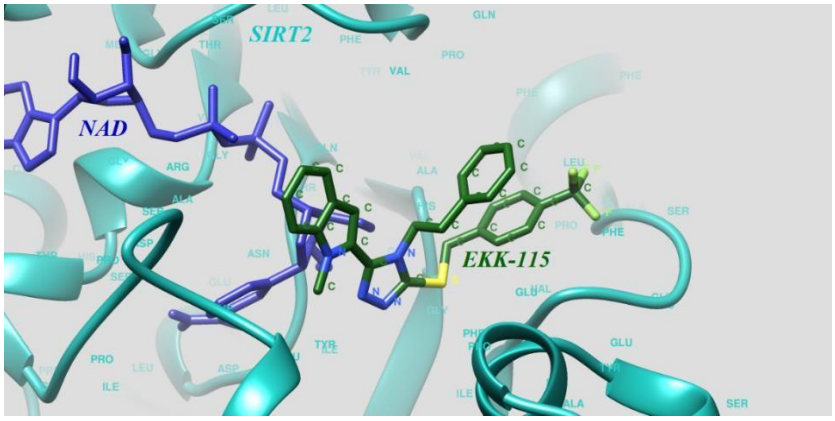

Figure 4.2.2.2: Visualization of molecular docking of the compounds to Sirt2. Docking of Sirt2 to **A.** SiReal2 **B.** EK-79 **C.** EK-99 **D.** EK-101, and **E.** EKK-115 in the presence of NAD^+ cofactor. (Figures created in Chimera 1.15 RC)

According to the best docking pose images (Figure 4.2.2.2) and free binding energies (Table 4.2.2.2), the compounds interact with Sirt2 but are not as strong as Sirt1 (Table 4.2.2.1). DEEPScreen analysis revealed that EK-79, EK-99, and EK-101 interact with Sirt2 with %80 accuracy (Table 4.2.1); however, it was not robustly proved by molecular docking.

Table 4.2.2.2: The estimated free binding energies for molecular docking of the compounds to Sirt2

Compound	Binding energy
SiReal2	ΔG= -7.12 kcal/mol
EK-79	ΔG= -7.75 kcal/mol
EK-99	ΔG= -6.80 kcal/mol
EK-101	ΔG= -7.78 kcal/mol
EKK-115	ΔG= -6.68 kcal/mol

4.2.3 Structural similarity between the compounds and the positive control

Since both DEEPScreen and Autodock4 results suggested the interactions of the compounds to Sirt1 with high confidence, further studies primarily focused on Sirt1-related mechanisms. A positive control, EX-527 (Selisistat), as the Sirt1 binding molecule was selected in these studies. An online tool was utilized to reveal how the potent compounds were structurally similar to EX-527 (https://chemminetools.ucr.edu/) (Backman et al., 2011). The compounds shared approximately %25 of their chemical structure with EX-527 (Table 4.2.3). This standard structure can be indole itself.

Table 4.2.3: MCS Tanimoto coefficient within the compounds

	EK-79	EK-99	EK-101	EKK-115	EX527
EK-79	1	0.72	0.77	0.72	0.24
EK-99	0.72	1	0.54	0.7	0.25
EK-101	0.77	0.54	1	0.55	0.24
EKK-115	0.72	0.7	0.55	1	0.24
EX-527	0.24	0.25	0.24	0.24	1

Structural similarity between the compounds and EX-527 revealed that the molecules do not resemble chemically and structurally. However, discovering a novel compound that does not have similarities is considered a possible advantage in terms of its uniqueness in the mechanism of action.

4.3 In vitro validation of Sirt1 targeting of the compounds

With the investigation and the determination of the compounds' target(s) via *in silico* methods (Part 4.2), in this part, *in vitro* validation of the compounds targeting Sirt1 mechanisms is explained.

4.3.1 Localization of Sirt1 in HCC cells

Sirt1 mainly functions in nuclear compartments, yet, it can relocate itself to the cytoplasm (Yanagisawa et al., 2018). To clarify the basal amount of Sirt1 in the nuclear and cytoplasmic regions of two representative HCC cells (Huh7 and SNU475), nuclear and cytoplasmic proteins were first extracted separately (Figure 4.3.1.1). In SNU475 cells, extraction of nuclear and cytoplasmic regions was more apparent (Figure 4.3.1.1B) than Huh7 cells (Figure 4.3.1.1A).

A.

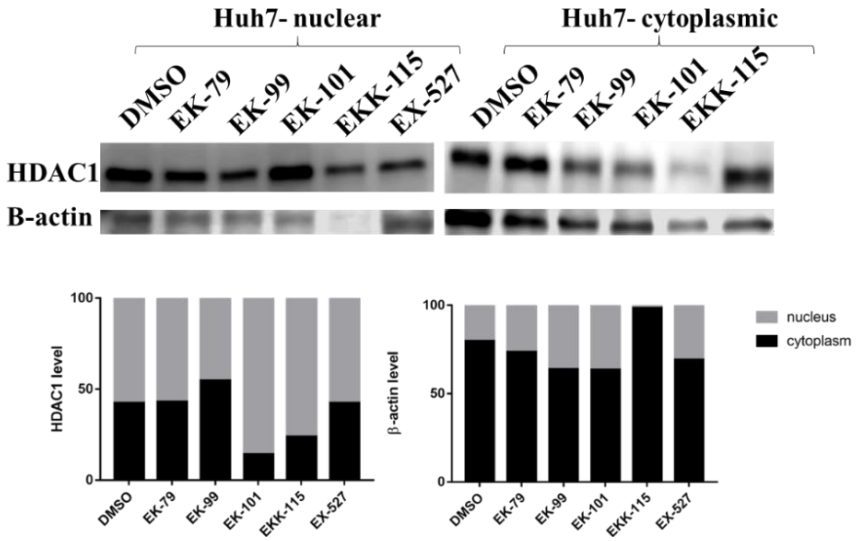

B.

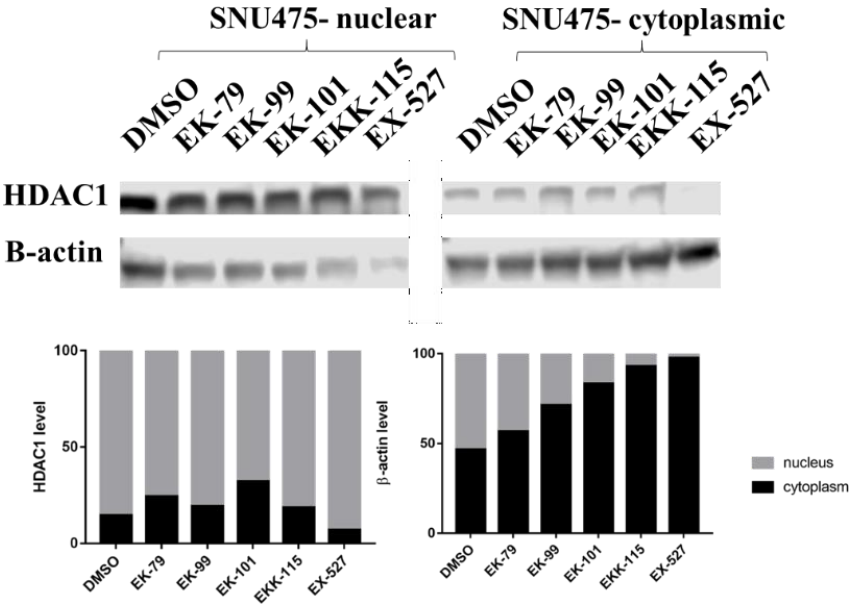

Figure 4.3.1.1: The separation of nuclear and cytoplasmic proteins. A. Nuclear (HDAC1) and cytoplasmic (β- actin) protein controls after the extraction of Huh7 cells. **B.** Nuclear (HDAC1) and cytoplasmic (β- actin) protein controls after the extraction of SNU475 cells.

Although the main compartmentalization of Sirt1 is the nucleus, according to ELISA results, the cytoplasmic fraction of both Huh7 and SNU475 cells contained more Sirt1, which has a tumor-suppressive role in the cytoplasm of HCC cells (Mao et al., 2014) (Figure 4.3.1.2). The localization of Sirt1 was investigated in protein expression level with the Western Blot experiment (Figure 4.3.1.2B). Thus, the two works supported each other.

Additionally, one of the most crucial targets of Sirt1, which is the p53 acetylation level, was observed with the Western Blot (Figure 4.3.1.2B). There was basal level acetyl p53 in cancerous cells even in the presence of Sirt1 (Figure 4.3.1.2B-C). The acetyl p53 basal presence might be related to the other factors/proteins affecting acetylation modification on p53.

The results might also be affected by the efficient nuclear-cytoplasmic separations.

A.

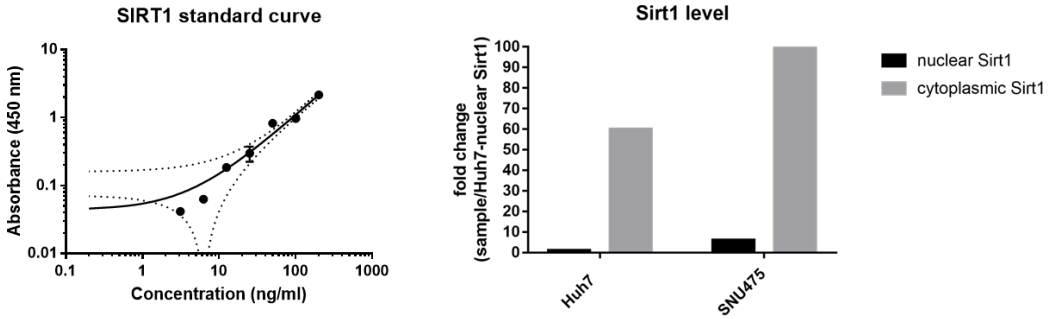

B.

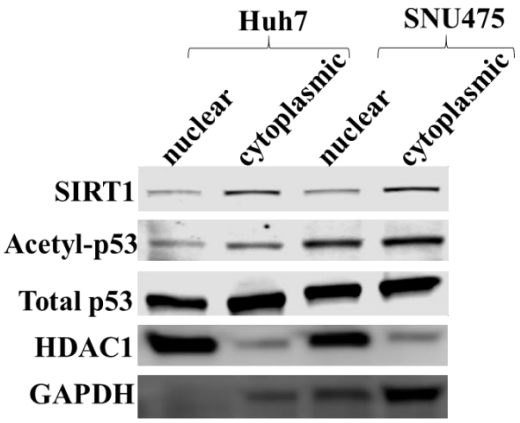

C.

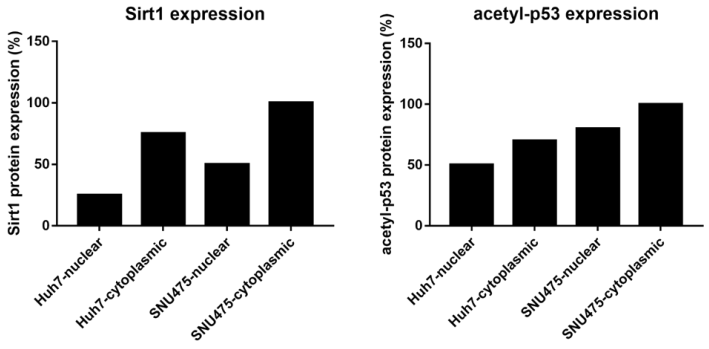

Figure 4.3.1.2: Determination of the amount of nuclear and cytoplasmic Sirt1 level in HCC cells. A. In bar graphs, Sirt1 amount (fold change according to Huh7-nuclear Sirt1 concentration) in Huh7 and SNU475 cells was shown. Sirt1 standard curve for ELISA assay was shown on the left. **B.** The conformation of Sirt1 level in Western Blot experiment. **C.** The normalization of the intensities was done according to loading controls.

4.3.2 Changes in HCC Sirtuin activity induced by the compounds

Universal Sirt Activity assay was utilized in the nuclear fraction of SNU475 and Huh7 to examine how the novel compounds influence Sirtuin enzymatic activity. In Huh7 cells, the inhibition capacity of EK-99, EK-101 and EKK-115 was robust in the nuclear Sirtuins (Figure 4.3.2.1A). To further validate these results in protein level, acetyl-53 expression was examined in the Western Blot experiment (Figure 4.3.2.1B). Acetyl-p53 increase in the presence of EK-99, EK-101, and EKK-115 compounds in Huh7 was similar to Sirtuin inhibition capacity (Figure 4.3.2.1).

A.

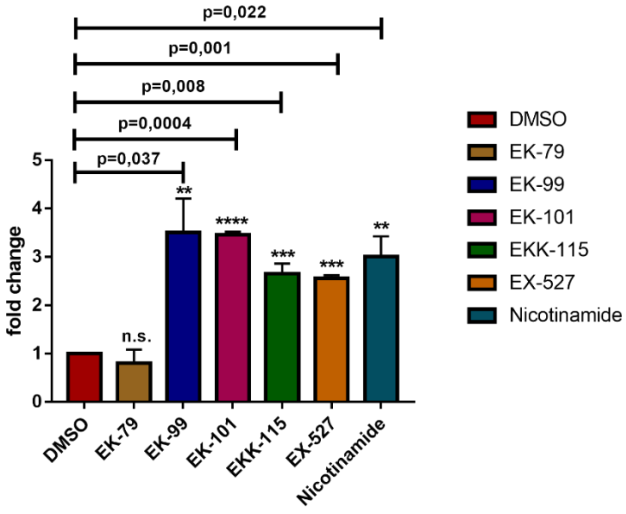

B.

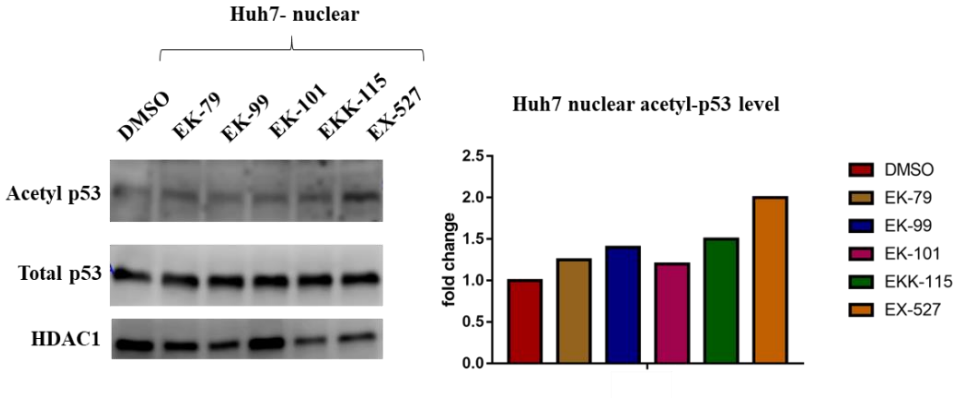

Figure 4.3.2.1: Investigation of the Sirtuin activity in Huh7 cells. A. Sirtuin inhibition in the nuclear fraction of Huh7 cells.IC_{100} concentrations were used, and nicotinamide was a positive control (n=2). **B.** Acetyl-p53 expression level upon the compound treatments (IC_{100} concentrations, 48 hours) in the nuclear fraction of Huh7 cells.

In SNU475 cells, EK-79, EK-99 and EK-101 strongly inhibited nuclear Sirtuin activity, even more than the positive controls (Figure 4. 3.2.2A). However, acetyl-p53 was increased in all treatment groups up to 2 fold (Figure 4.3.2.2B).

A.

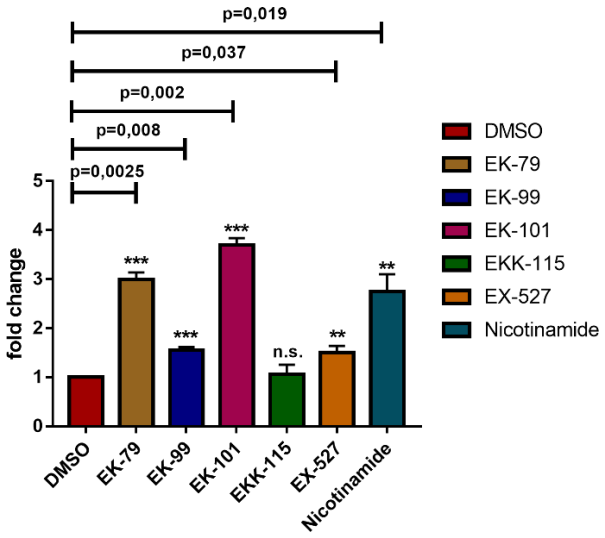

B.

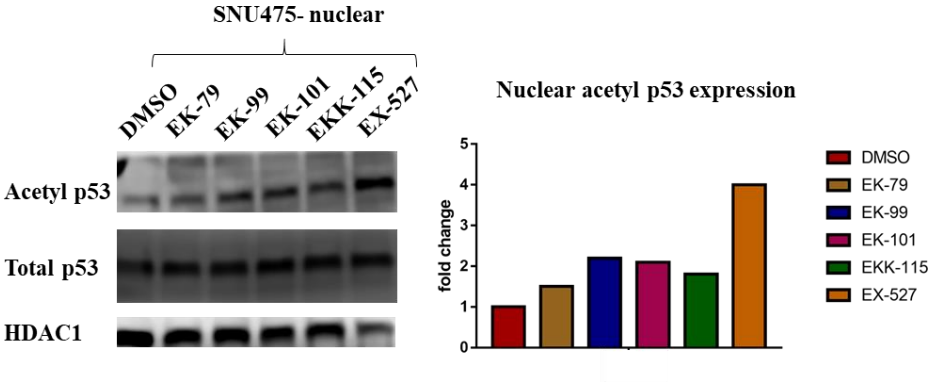

Figure 4.3.2.2: Investigation of the Sirtuin activity in SNU475 cells. A. Sirtuin inhibition in the nuclear fraction of SNU475 cells. IC_{100} concentrations were used, and nicotinamide was a positive control (n=2). **B.** Acetyl-p53 expression level upon the compound treatments (IC_{100} concentrations, 48 hours) in the nuclear fraction of SNU475 cells. HDAC1 was the nuclear loading control. Bar graphs indicate a normalization of the expression level of acetyl-53 according to loading control.

4.4 The cytotoxicity of the selected compounds against HCC

In this part, the cytotoxicity of the chosen four molecules with the positive control was investigated. The potency of the molecules for interfering with HCC cell survival was studied. In this scope, the profile of proliferation, cell death, cell cycle of HCC cells was examined upon the molecules treatment.

4.4.1 Cytotoxic activity of the potent compounds against HCC panel

The positive control EX-527 and the compounds EK-79, EK-99, EK-101, EKK-115 cytotoxicity were investigated against five different HCC cell lines.

The SRB experiments were repeated at different times throughout the study. Table 4.4.1 represents the average of all the IC_{50} values calculated from each SRB experiment.

The concentrations were an indicator for the cytotoxicity against HCC cells. The growth inhibition capacity of the molecules was also promising (Supplementary Figure 1).

Table 4.4.1: IC_{50} (μM)* values of selected indole derivatives on Huh7, SNU475, Mahlavu, HepG2, and Hep3B-TR cells via SRB assay, after 72 hours treatment.

Compound	Huh7	SNU475	Mahlavu	HepG2	Hep3B-TR
EK-79	4.8	8.9	13.1	7.4	8.8
EK-99	2.0	9.3	10.5	6.7	3.4
EK-101	4.2	13.2	10.8	7.6	6.7
EKK-115	5.1	6.4	3.2	3.4	5.3
EX-527	3.4	13.0	21.3	14.1	24.3

*R^2 values were within the range of 0.75 to 0.99 for each value. The experiment was performed as technical replicates and biological replicates.

Apart from HCC cells, non-cancer MCF-12A cell viability was also studied as negative control (Figure 4.4.1.2). The IC_{50} concentrations of the compounds on normal-like cells were much higher than the concentrations effective on cancer cells.

A.

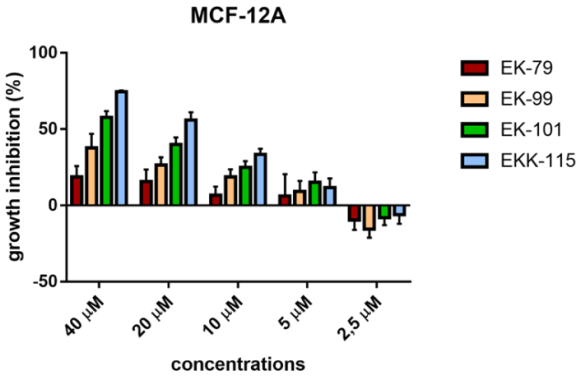

B.

	IC_{50} (µM)
EK-79	>40 µM
EK-99	>40 µM
EK-101	29,0 µM
EKK-115	17,2 µM

Figure 4.4.1.2.: IC50 (µM) values of selected indole derivatives on non-cancer MCF-12A cells A. Growth inhibition capacity of the compounds in 72 hours. **B.** Calculated IC_{50} (µM) concentrations in 72 hours (R^2 values were within the range of 0.9 to 0.99 for each value. The experiment was performed as triplicates.).

Huh7 and SNU475 cells were used as representative epithelial and mesenchymal-like (H et al., 2009) HCC cells, respectively, for the following experiments.

4.4.2 Real-time proliferation observation of HCC cells upon the compounds

RT-CES technology was utilized to monitor real-time HCC cell proliferation, treated with EK-79, EK-99, EK-101, and EKK-115. Compounds were given in increasing concentrations determined based on the previously performed SRB experiments for Huh7 and SNU475 cells. DMSO was used as a negative control to compare proliferative activity to treatment groups in 72 hours. There was a

significant growth inhibition of each HCC cell line upon the compound treatment compared to DMSO (Figure 4.4.2.1).

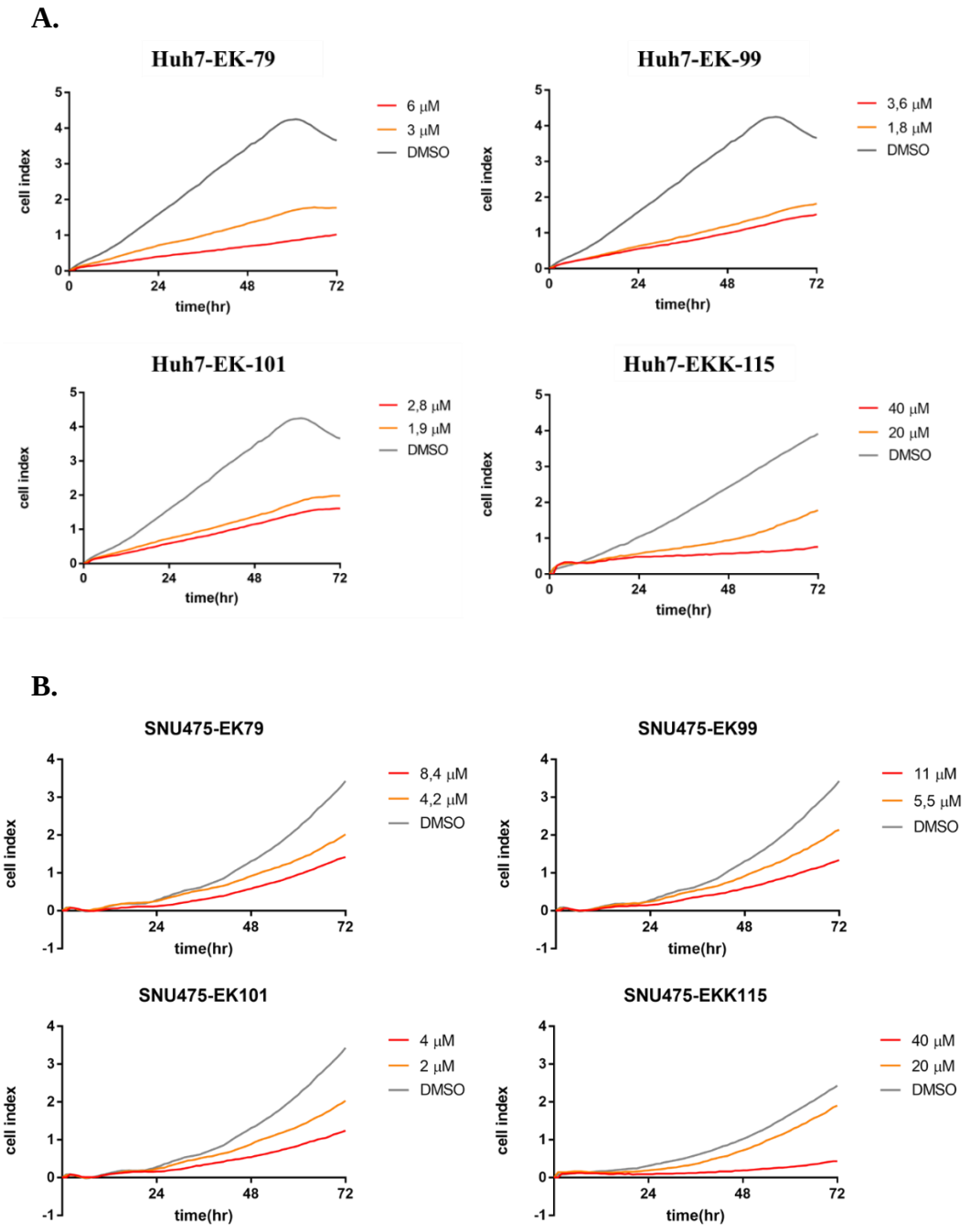

Figure 4.4.2.1: Real-time observation of the proliferation of HCC cells treated with the selected compounds. HCC cell lines such as Huh7 (A), SNU475 (B),

growth curves in 72 hours. The experiment was performed in triplicates, and the results were represented as the average of all replicates.

Based on the percent inhibition vs. concentration curves generated from the normalized cell index values of treatment and control groups (Figure 4.4.2.1), the IC_{50} doses for 72 hours were calculated. The results are shown in Table 4.4.2. Compared to the SRB results, the IC_{50} values calculated from the RT-CES experiments were found more reliable. This is because the sensitivity and accuracy of this system are much higher (eliminating technical-induced variance), unlike SRB assay, which is cruder (R et al., 2012).

Table 4.4.2: The effective doses based on the real-time proliferation curves

	IC_{50} (based on RT-CES analysis)	
Compound	**Huh7**	**SNU475**
EK-79	6.0 μM	9.5 μM
EK-99	3.6 μM	10.4 μM
EK-101	6.5 μM	15.2 μM
EKK-115	9.3 μM	14.1 μM

Mahlavu, HepG2 and Hep3B-TR cells also showed a similar response to the compounds for cell proliferation (data not shown).

The cell proliferation profile of the treated HCC cells promisingly suggests that the compounds induce cell death or cell cycle arrest in HCC cells. Therefore, further investigations were focused on these two phenomena of cancer.

4.4.3 The morphological changes of the HCC cells upon the treatment

To monitor the appearance of the cells treated with the molecules, observations under the light microscope were done for 12, 24, 36, 48 and 72 hours (supplementary figures 2 and 3). For the treatment, the IC_{100} doses considering the RT-CES analysis

results were used. Since after 24 hours, cells start to dye or proliferate slowly, it was set as the time point for further experiments.

4.4.4 Potential cell death mechanisms in HCC triggered by the compounds

The apoptotic capacity of the indole derivatives for Huh7 cells was first monitored with Hoechst 33258 staining. Nuclear blebbing is the form of fragmented DNA that occurs at the end of apoptosis (*In Fight against Cancer, a Closer Look at Nuclear Blebbing -- ScienceDaily*, n.d.) and can be observed with the staining. Fragmented DNA and nuclear blebbing were observed with all the treatment groups in 24 hours (Figure 4.4.4.1A). Representative images for the other time points are given in supplementary figure 4.

Flow cytometric analysis was conducted to detect early and late apoptotic cell proportions of Huh7 and SNU475 cells in response to the compounds. After 24 hours of treatment of the cells, in Huh7 cells, EK-79, EK-99, and EK-101 compounds increase the FITC positive cells by forcing the cells to apoptosis. (Figure 4.4.4.1B-C). Doxorubicin is a well-known chemotherapeutic agent in HCC that induces apoptosis and is used as a positive control.

A.

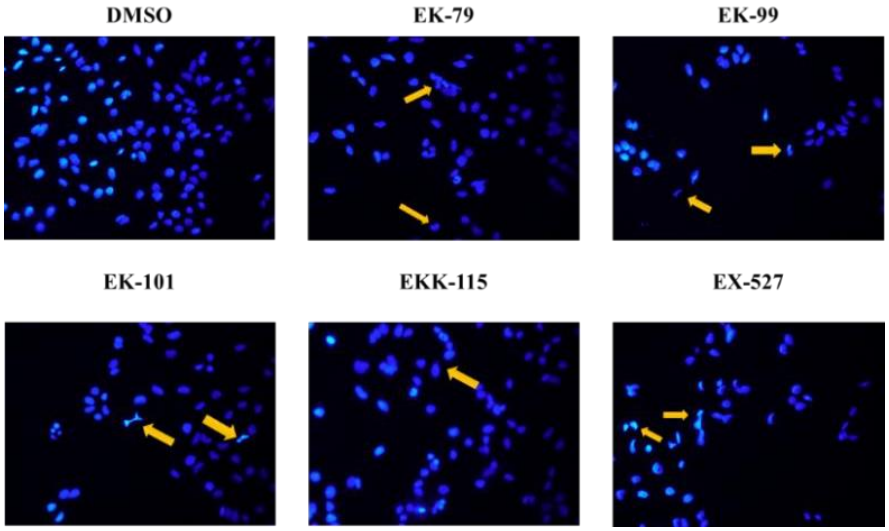
DMSO
EK-79
EK-99
EK-101
EKK-115
EX-527

B.

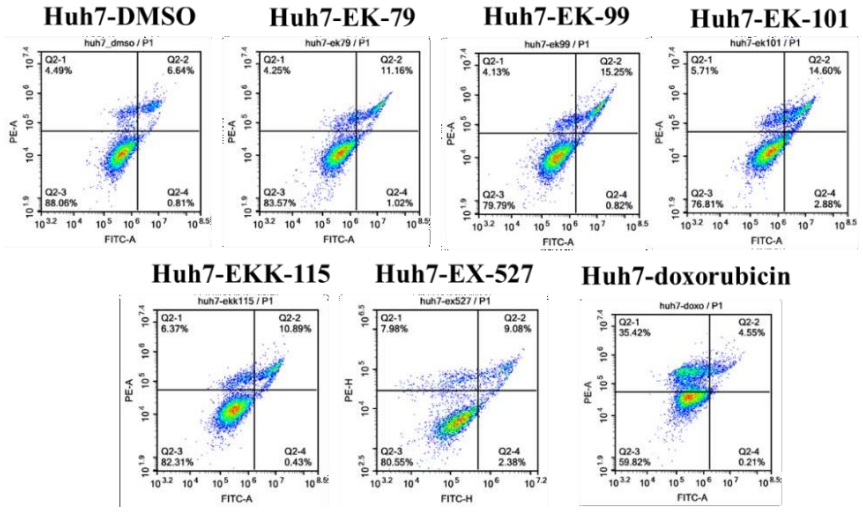
Huh7-DMSO
Huh7-EK-79
Huh7-EK-99
Huh7-EK-101
Huh7-EKK-115
Huh7-EX-527
Huh7-doxorubicin
PE-A
FITC-A
PE-H
FITC-H

C.

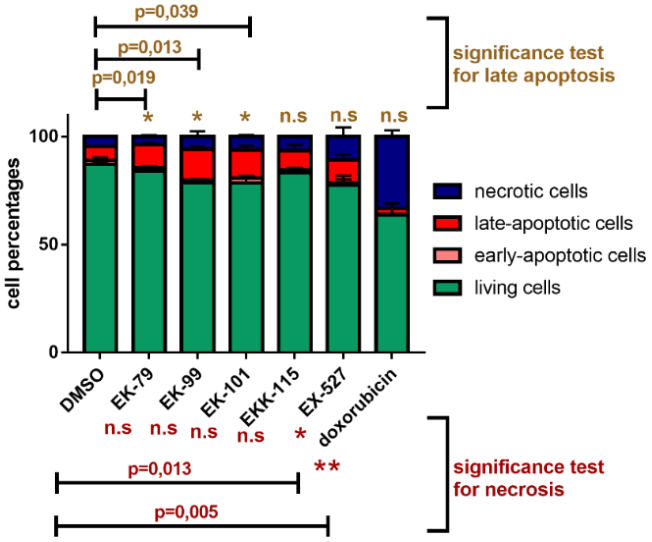

Figure 4.4.4.1: Investigation of cell death mechanisms in Huh7 cells. A. Hoechst images of treated Huh7 cells for 24 hr. Nuclear blebbing was shown with yellow arrows. **B.** Flow cytometry analysis of Annexin V assay, the concentration of the compounds is $IC_{100,}$ and treatment time is 24 hours. Q2-1 quadrant represents propidium iodide (PI)+/annexinV- necrotic cells; Q2-2 quadrants represents PI+/annexinV+ late apoptotic cells; Q2-3 represents PI-/annexinV+ early apoptotic cells; Q2-4 quadrant represents PI-/annexinV- live cells. Images were representative of 2 independent biological replicates. **C.** Statistical analysis Huh7 cells with treatment and control group (n=2, Student t-test, $p<0.05$).

Western Blot experiment was also conducted to observe the expression of apoptotic proteins in Huh7 cells. PARP is a family of proteins functioning in DNA repair, genomic stability, and apoptosis. 89 kDa cleaved fragment of PARP is catalytically active and has a role in apoptotic cell death (Chaitanya et al., 2010). In Huh7 cells, EK-101 led to PARP cleavage similar to the positive control to trigger apoptosis (Figure 4.4.4.2).

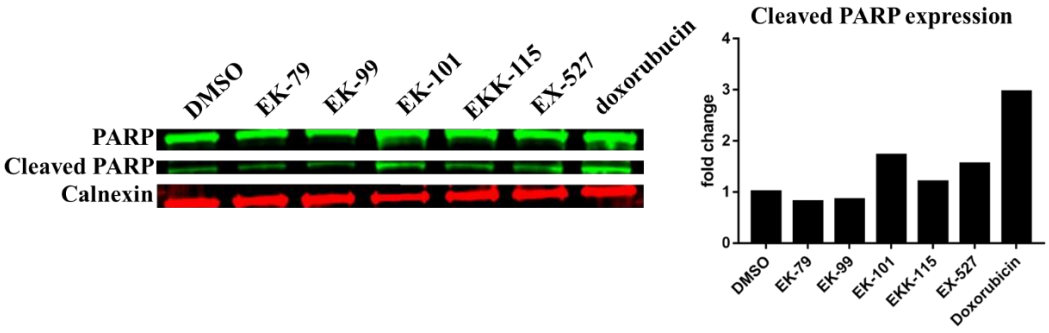

Figure 4.4.4.2: Western blot analysis with apoptotic proteins in Huh7 cells. Cells were treated with the IC_{100} concentration of the compounds for 24 hours. Calnexin is the loading control, and the bar graph represents the fold change.

The cell death response of SNU475 induced by the compounds was shown in Figure 4.4.4.3 and supplementary figure 5. All of the compounds triggered SNU475 cells to undergo apoptosis. In addition to apoptosis, the EK-101 molecule caused necrosis to the cells (Figure 4.4.4.3C).

A.

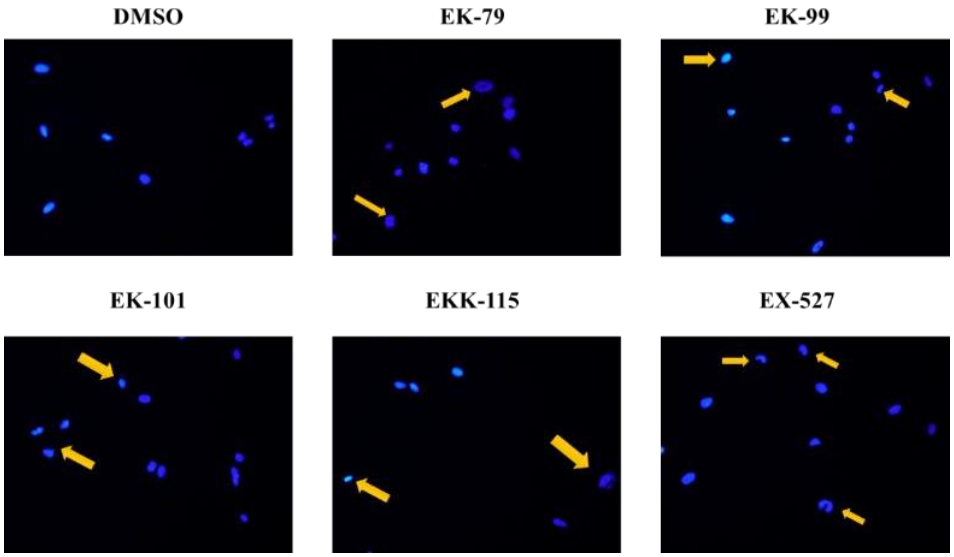

B.

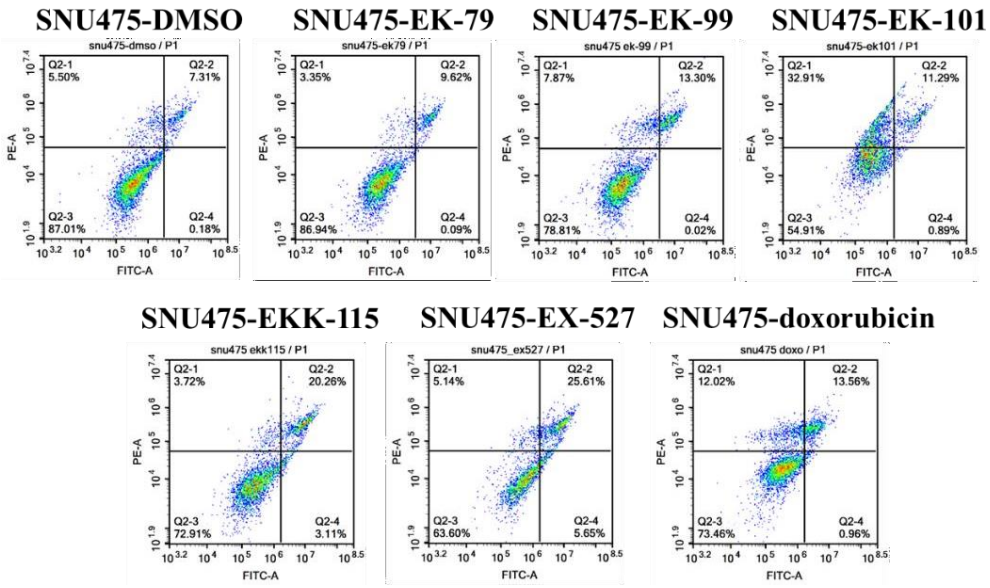

C.

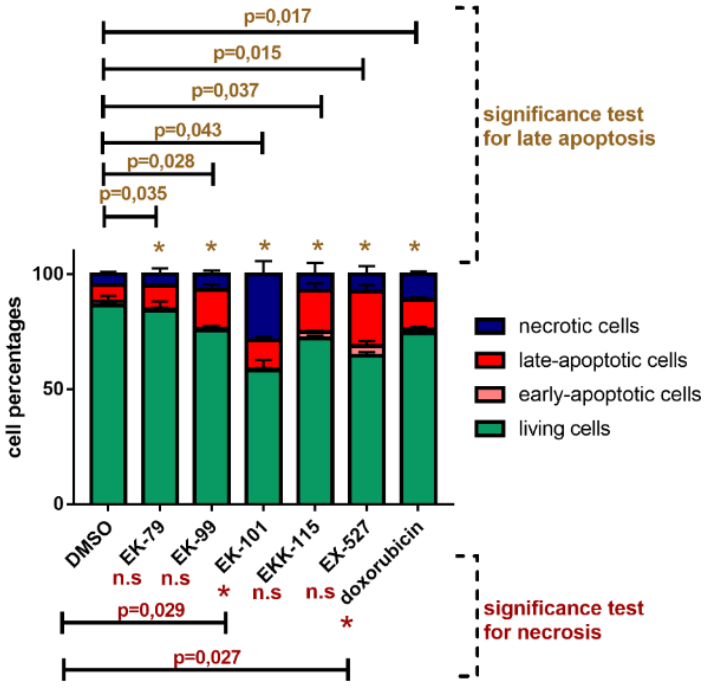

Figure 4.4.4.3: Investigation of cell death mechanisms in SNU475 cells. A. Hoechst staining of treated SNU475 cells for 24 hours. **B.**Flow cytometry analysis of Annexin V assay, the concentration of the compounds is IC_{100}, and treatment time is 24 hours. Q2-1 quadrant represents propidium iodide (PI)+/annexinV- necrotic

cells; Q2-2 quadrants represents PI+/annexinV+ late apoptotic cells; Q2-3 represents PI-/annexinV+ early apoptotic cells; Q2-4 quadrant represents PI-/annexinV- live cells. **B.** Graphical representation of the annexin V assay of SNU475 cells with treatment and control groups. **C.** Statistical test for apoptosis and necrosis (n=2, Student's t-test)

All compounds increased PARP cleavage in SNU475 cells (Figure 4.4.4.4).

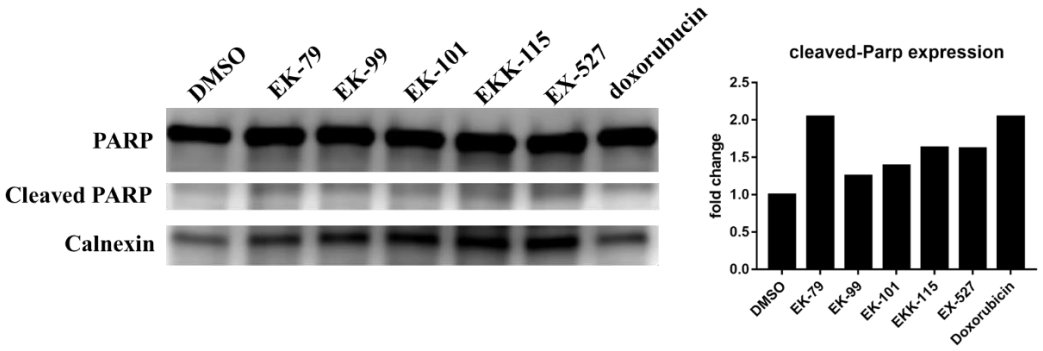

Figure 4.4.4.4: Western blot analysis with apoptotic proteins. Cells were treated with the IC_{100} concentration of the compounds for 24 hours. Calnexin is the loading control, and the bar graphs represent the fold change of cleaved PARP expression according to the negative control.

Overall, the compounds can stimulate cell death in the form of apoptosis or necrosis.

4.4.5 Cell Cycle Profile of HCC cells upon the compound treatments

Previous parts proved that the compounds were cytotoxic to HCC cells, decreased proliferation, or stimulated cell death. To examine whether this growth inhibition was due to cell cycle arrest or not, cell cycle analysis with PI stain was performed. In Huh7 cells, all the compounds led to significant G1 arrest compared to DMSO negative control (Figure 4.4.5.1).

A.

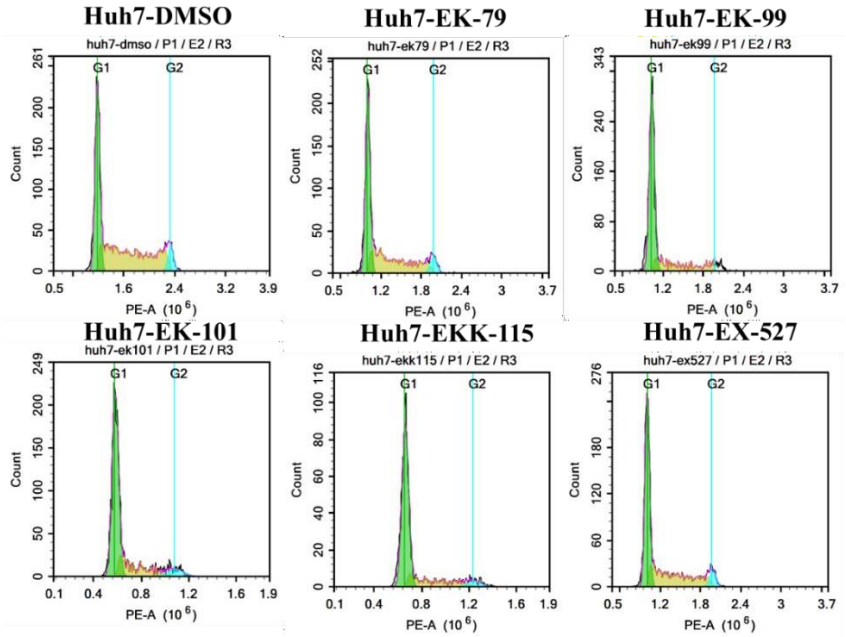

B.

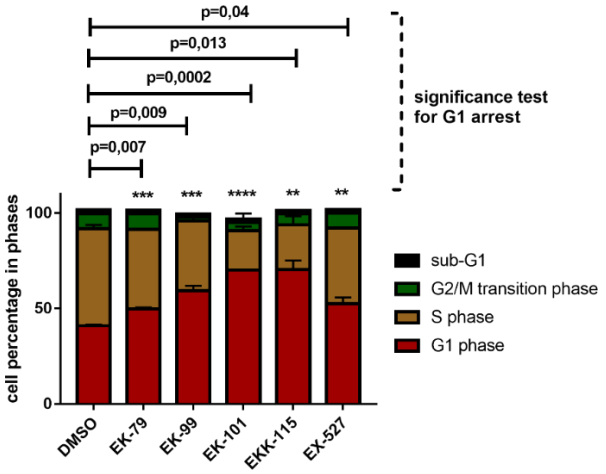

Figure 4.4.4.1: Cell cycle analysis of the Huh7 cells by flow cytometry. A. Representative flow cytometry images for Huh7 cells. **B.** Statistical test for analysis of Huh7 with 24 hours treatment of the compounds (n=2, Student's t-test for G1 phase, $p<0.05$)

For SNU475 cells, except for EK-99, all the molecules led to G1 arrest (Figure 4.4.4.2).

A.

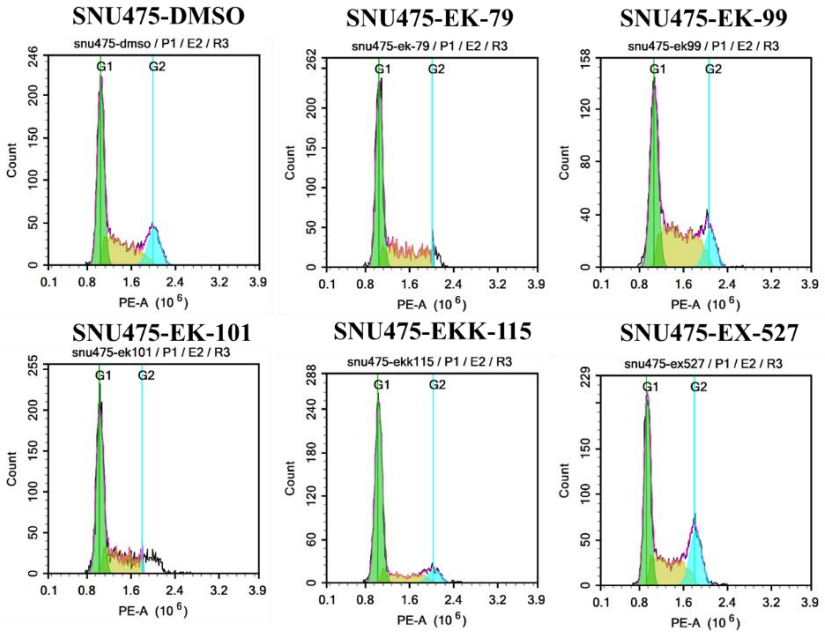

B.

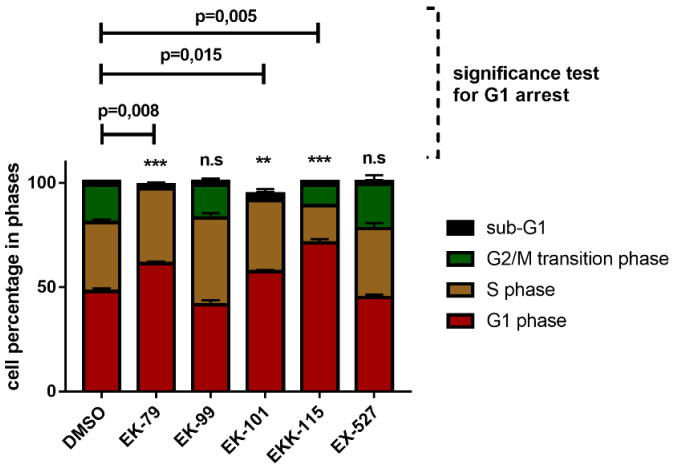

Figure 4.4.4.2: Cell cycle analysis of the SNU475 cells by flow cytometry. A. The flow cytometry images for SNU475 cells. **B.** Graphical representation for SNU475 cell cycle profile (upon IC_{100} concentrations of the compound treatments for 24 hours (n=2, Student's t-test for G1 phase, $p<0.05$)

According to these results, the selected indole derivatives were cytotoxic to cells and inhibited the growth of HCC or led to cell death to interfere with the tumorigenesis.

DISCUSSION

5.1 Target Assessment

Discovering new compounds is essential for many researchers working in cancer therapeutics because cancer is still difficult to cure in many patients. Due to the high cost and labor-intensive nature of *in vitro* and *in vivo* experiments, it has become crucial to use machine learning-based tools to predict the possible targets of novel compounds *in silico* before revealing their mechanism of action. In this thesis, both drug target prediction methods and *in vitro* experiments are utilized to study the effects of novel indole derivatives on HCC cell lines.

These novel indole derivatives were synthesized by mimicking Sirtuin inhibitors. With this knowledge from the synthesizer, Professor Sultan Baytaş, we first checked whether these molecules were cytotoxic to three representative cancer cell lines. Indeed, the molecules effectively killed or inhibited the growth of colon cancer HCT116, breast cancer MCF7 and hepatocellular carcinoma Huh7 cell lines with acceptable IC_{50} concentrations. Then, according to Sultan Baytaş's consultant, they were chosen to be potent based on their IC_{50} values and structure-activity relationships.

Further studies were performed with these selected molecules, which are EK-79, EK-99, EK-101, and EKK-115. After investigating their anti-cancer property, the DEEPScreen database was utilized to predict whether these selected molecules target Sirtuin proteins. The molecules were predicted to interact with Sirt1 and Sirt2 yet Sirt3 in a computer environment with high accuracy. Sirt1, Sirt2, and Sirt3 catalytic domains share 55% sequence similarity, and they arose from the same ancestor, as seen in Figure 5.1.1.

Figure 5.1.1: The alignment tree of all isoforms of the Sirtuin family. Among all the seven isoforms, based on the sequence alignment of the catalytic domains, Sirt1, Sirt2, and Sirt3 are more homologous than others (in red rectangle).

Although Sirt1, Sirt2 and Sirt3 resemble well, the DEEPScreen results hit only Sirt1 and Sirt2. It might be related to the difference of 45% in the catalytic domains. Also, Sirt1 and Sirt2 catalytic domains share 66.5% sequence similarity (Figure 5.1.2); the compounds may fit best to the structure formed by this 66.5% similar sequence.

```
Q96EB6 SIR1_HUMAN  241  NTIEDA--VKLLQECKKIIVLTGAGVSVSCGIPDFRSRD-GIYARLAVDFPDLPDPQAMF  297
Q8IXJ6 SIR2_HUMAN   62  LTLEGVARYMQSERCRRVICLVGAGISTSAGIPDFRSPSTGLYDNL--EKYHLPYPEAIF  119
                         *:*..      :.*:::* *.***:*.*.******* . *:* .*  :  .** *:*:*

Q96EB6 SIR1_HUMAN  298  DIEYFRKDPRPFFKFAKEIYPGQFQPSLCHKFIALSDKEGKLLRNYTQNIDTLEQVAGIQ  357
Q8IXJ6 SIR2_HUMAN  120  EISYFKKHPEPFFALAKELYPGQFKPTICHYFMRLLKDKGLLLRCYTQNIDTLERIAGLE  179
                         :*.**:*.*.*** :***:*****:*::** *: * ..:* *** *********::**::

Q96EB6 SIR1_HUMAN  358  --RIIQCHGSFATASCLI--CKYKVDCEAVRGDIFNQVVPRCPRCPADEPLAIMKPEIVF  413
Q8IXJ6 SIR2_HUMAN  180  QEDLVEAHGTFYTSHCVSASCRHEYPLSWMKEKIFSEVTPKCEDCQ-----SLVKPDIVF  234
                            :::.**:* *: *:   *:::   . :: .**.:*.*:*  *      :::**:***

Q96EB6 SIR1_HUMAN  414  FGENLPEQFHRAMKYDKDEVDLLIVIGSSLKVRPVALIPSSIPHEVPQILINREPLPHLH  473
Q8IXJ6 SIR2_HUMAN  235  FGESLPARFFSCMQSDFLKVDLLLVMGTSLQVQPFASLISKAPLSTPRLLINKEKAGQSD  294
                         ***.** :*. .*: *  :****:*:*:**:*:*.* : *. * ..*::***:*   : .

Q96EB6 SIR1_HUMAN  474  ----------------------FDVELLGDCDVIINELCHRLGGEYAKLCCNPVKLSEITE  512
Q8IXJ6 SIR2_HUMAN  295  PFLGMIMGLGGGMDFDSKKAYRDVAWLGECDQGCLALAELLGWKK--------ELEDLVR  346
                                              **  **:**     *.. ** :         :*.:::.
```

Figure 5.1.2: Sequence alignment of catalytic domains of Sirt1 and Sirt2. Yellow regions belong to the sequence of catalytic domains.

Additionally, all of these selected molecules, EK-79, EK-99, EK-101, and EKK-115, share 70% structural similarity, according to the ChemMine tool (Backman et al., 2011). A similar core with an indole ring in the molecules can fit the identical regions in catalytic domains of Sirt1 and Sirt2. When the chemical structure of the molecules is investigated in detail (Figure 5.1.3), it is remarkable that they end up with $–CF_3$ radical, which can be important in the drug-target interaction. Trifluoromethyl radical ($-CF_3$) has unique chemical properties like increasing acidity, lipophilicity and metabolic stability of the rest chemical structure, so it is widely used in many drugs (Buwen et al., 2017).

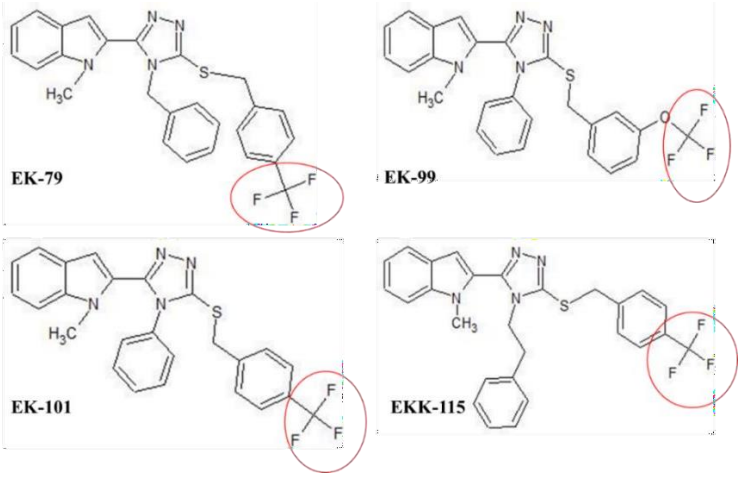

Figure 5.1.3: Chemical structures of EK-79, EK-99, EK-101, and EKK-115. Trifluoromethyl radical (-CF_3) is shown in red circles on the structures.

The selected molecules were docked to Sirt1 and Sirt2 proteins for further investigations to observe similar results with different *in silico* methods. Surprisingly, when estimated free binding energies were obtained, only the molecule docking to Sirt1 protein was similar to the DEEPScreen results. According to molecular docking studies via AutoDock4 software, Sirt2 can also interact with the molecules; however, Sirt1 data was more remarkable and robustly showed the interaction in the computer environment. That is why only Sirt1 was the main focus for the further studies.

For *in vitro* validation of *in-silico* results, nuclear and cytoplasmic fractions were extracted separately because the Sirt1 level differs in these compartments, targeting different proteins. The proteins were not strictly separated from nuclear and cytoplasmic ones, specifically for Huh7 cells. The compounds may interfere with the flexibility of the nuclear and cytoplasmic membranes or may change the expression of the control proteins. When Sirt1 levels are observed in these compartments, the results are against the literature because Sirt1 mainly locates itself to the nucleus. However, Sirt1 localization is dynamic; the moment of the extraction might give rise to these results. Also, the efficacy of the separation of the compartments may affect the results.

Nevertheless, since one of the main targets of Sirt1, p53, is an essential tumor suppressor for HCC, and its compartment is primarily the nucleus, only the nuclear regions of the samples were shown. Additionally, overexpression of cytoplasmic Sirt1 is related to more prolonged overall survival and tumor-suppressive effect in HCC patients (Mao et al., 2014). Yet, the results for the cytoplasmic fractions were not revealed. With total lysate, we would not clearly see the protein status in the nuclear compartment; therefore, with the extraction, we enriched the nuclear proteins of HCC cells.

According to Sirtuin enzymatic activity assay results, in Huh7 cells, EK-99, EK-101, EKK-115 inhibit nuclear Sirtuins Sirt1, Sirt3, Sirt6 or Sirt7. Also, all the molecules could increase the acetyl-p53 level, although not statistically proven. p53 is targeted only by Sirt1, not other sirtuin isoforms. Therefore, the compounds, which gave similar results in the enzymatic activity assay and western blot experiment, may claim that Sirt1 activity is inhibited via the compounds EK-99, EK-101, and EKK-115. Enzymatic activity is susceptible to environmental conditions; thus, the compatibility of western blot experiments and the activity assays may differ. When the docking and DEEPScreen results are revisited, EK-101 and EKK-115 were predicted to interact with Sirt1, not EK-99. The incompatibility of these different methods may also arise from our lack of knowledge of whether these molecules are selective for Sirt1 or interact with other targets. However, we might suggest that EK-101 and EKK-115 were both *in silico* and *in vitro* predicted to interact and affect Sirt1 in Huh7 cells. For SNU475 cells, EK-79, EK-99, and EK-101 molecules block nuclear sirtuins; all the molecules increase the acetyl-p53 level in this highly aggressive cell line (with lack of statistical analysis), and the *in silico* results are promising for EK-79 and EK-101.

5.2 Cytotoxicity Assessment

After dealing with the target investigation, the cytotoxicity of the selected molecules was studied in HCC cells. These selected molecules were examined for

their cytotoxicity on several HCC cells. The IC_{50} values of the molecules in different HCC cells, specifically p53-null Hep3B-TR cells (Schilling et al., 2010), showed us that these molecules are cytotoxic to the HCC, but not only via targeting Sirt1 to elevate p53 function. They interfere with the tumorigenesis of HCC via affecting different processes, which are waiting to be revealed.

Since SRB is a robust method and susceptible to many factors, the experiment was performed three times in different periods. IC_{50} concentrations differed in each experiment; therefore RTCES experiment was conducted to find out the effective doses. Moreover, SNU475 cells with mesenchymal-like features and Huh7 cells with epithelial markers were selected to investigate the effect of the molecules. Based on the cell index, new doses were calculated, and they were more or less similar. Also, the molecules are not toxic to non-cancer cells at their effective concentrations, suggesting that the compounds exhibit specificity for cancerous cells.

Time-dependent microscopy imaging and Hoechst staining were performed on these cells to understand when the compounds started exhibiting their cytotoxic effects. Two times the average of the doses obtained from RTCES and SRB experiments were used to see whether these values were practical or not. In general, after 24 hours, morphological and nuclear alterations were visible in HCC cells with these doses. In further experiments, these doses and 24 hour treatment time were used.

In Huh7 cells, EK-79, EK-99, and EK101 led to G1 arrest and apoptosis after 24 hours. Specifically for EK-101, it interacts with Sirt1 *in silico*, inhibits Sirt1 activity and increases active (acetyl) p53 expression. Overall, re-activation of p53 upon EK-101 treatment may also contribute to G1-mediated apoptosis in Huh7 cells. Other molecules also interfere with the tumorigenesis of Huh7, yet with different mechanisms.

In SNU475 cells, all the molecules trigger cells to undergo apoptosis and arrest the cell cycle at the G1 phase. Together with that, EK-79, EK-99, and EK-101 block

Sirt1 activity and elevate acetyl-53 level, suggesting p53-drived G1 arrest-mediated apoptosis with an acceptable probability. For EK-79 and EK-101, it was supported by *in silico* predictions as well. Besides that, EK-101 causes necrosis in these aggressive cells, which needs further attention and experimental research to understand its mechanism of action in more detail.

5.3 Summary

In summary, since the newly synthesized molecules were novel and unknown, their targets were predicted with several *in silico* methods. It was revealed that they might interact with Sirt1 with high affinity in the computer environment. Sirt1 is overexpressed in HCC and promotes tumorigenesis for cancer cell survival. All the molecules behaved differently in various HCC cells to prevent tumorigenesis, but EK-101 was predicted to interact with Sirt1 in two different *in silico* methods. It was supported *in vitro* in both Huh7 and SNU475 cells. It needs to be further studied due to its high potency against HCC cells. The summary figure can be seen in Figure 5.3.

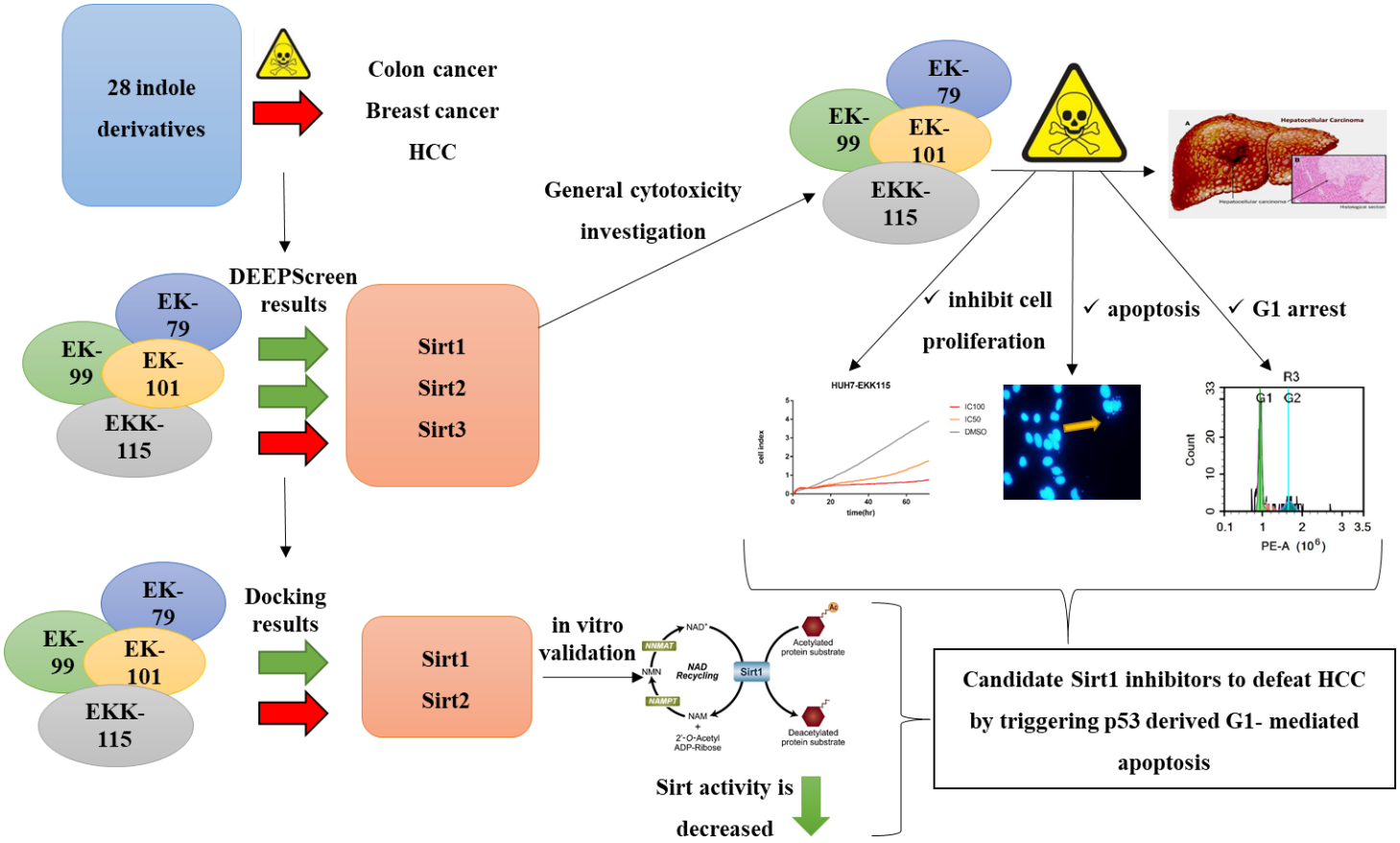

Figure 5.3: Summary of this study. The study starts with in silico methods (DEEPScreen and molecular docking) followed by in vitro results. Next, the cytotoxicity of the compounds is studied with HCC cells to monitor the effects of Sirt1 inhibition.

FUTURE PERSPECTIVES

Although the DEEPScreen and AutoDock4 software were reliable enough to assess the compounds robustly, virtual screening for all known proteins can be performed for all possible targets of the compounds. Also, RNA-sequencing or NanoString studies could be used to detect changes in the cell lines upon the molecule treatment to predict possible mechanisms of action.

For in vitro validation of Sirt1 targeting, only one enzymatic assay was utilized, which measures all isoforms of the Sirtuin family. An enzymatic assay that measures only Sirt1 activity must be used to have more reliable results. Also, the molecules can be biotinylated for immunoprecipitation experiments with Sirt1 and acetyl-p53. At the protein level, only acetyl-p53 expression was studied in western blot experiments. However, many other targets of Sirt1 are available, such as PTEN, FOXO3a, GSKα/β, β-catenin, NFκB and histone H3 and H4. Their acetylation status should be investigated with respective antibodies.

p53 is an essential protein that can be acetylated and deacetylated by other enzymes. If p53 is continued to be studied to investigate Sirt1 inhibition activity of the molecules, other HDACs and HATs should be considered that target p53. The p-53 signaling pathway with its downstream and upstream effectors should be studied in detail. Also, to show direct interaction of Sirt1 inhibition and acetyl-p53 elevation via the compounds, p53 null cell line Hep3B-TR or p53 knockout in other cell lines should be used as a negative control.

Additionally, only EX-527 was used as a positive control, which is a Sirt1 inhibitor. Another Sirt1 inhibitor, like Sirtinol, or as a negative control, Sirt1 activator resveratrol must be used to have more controls to make significant comparisons.

There were 28 molecules to study at first. To handle the search better, the eliminations of the molecules and cell lines were done; however, other molecules could also be effective in targeting Sirt1; or they can act better in different cell lines. That is why eliminated molecules and cell lines should be considered, too. Also, the chemical properties of the compounds should be determined, such as membrane permeability, nuclear localization signals, solubility and movement inside the cell, acidity, half-life, etc. New compounds can be designed and synthesized considering the structure-activity relationship of the potent compounds studied in the context of this thesis.

REFERENCES

Al-Bahrani, R., Tuertcher, D., Zailaie, S., Abuetabh, Y., Nagamori, S., Zetouni, N., Bahitham, W., & Sergi, C. (2015). Differential SIRT1 expression in hepatocellular carcinomas and cholangiocarcinoma of the liver. *Annals of Clinical and Laboratory Science*, *45*(1), 3–9.

Ally, A., Balasundaram, M., Carlsen, R., Chuah, E., Clarke, A., Dhalla, N., Holt, R. A., Jones, S. J. M., Lee, D., Ma, Y., Marra, M. A., Mayo, M., Moore, R. A., Mungall, A. J., Schein, J. E., Sipahimalani, P., Tam, A., Thiessen, N., Cheung, D., … Laird, P. W. (2017). Comprehensive and Integrative Genomic Characterization of Hepatocellular Carcinoma. *Cell*, *169*(7), 1327-1341.e23. https://doi.org/10.1016/j.cell.2017.05.046

Audrito, V., Vaisitti, T., Rossi, D., Gottardi, D., D'Arena, G., Laurenti, L., Gaidano, G., Malavasi, F., & Deaglio, S. (2011). Nicotinamide blocks proliferation and induces apoptosis of chronic lymphocytic leukemia cells through activation of the p53/miR-34a/SIRT1 tumor suppressor network. *Cancer Research*, *71*(13), 4473–4483. https://doi.org/10.1158/0008-5472.CAN-10-4452

Backman, T. W. H., Cao, Y., & Girke, T. (2011). ChemMine tools: An online service for analyzing and clustering small molecules. *Nucleic Acids Research*, *39*(SUPPL. 2). https://doi.org/10.1093/nar/gkr320

Bannister, A. J., & Kouzarides, T. (2011). Regulation of chromatin by histone modifications. In *Cell Research* (Vol. 21, Issue 3, pp. 381–395). Nature Publishing Group. https://doi.org/10.1038/cr.2011.22

Brunet, A., Sweeney, L. B., Sturgill, J. F., Chua, K. F., Greer, P. L., Lin, Y., Tran, H., Ross, S. E., Mostoslavsy, R., Cohen, H. Y., Hu, L. S., Cheng, H. L.,

Jedrychowski, M. P., Gygi, S. P., Sinclair, D. A., Alt, F. W., & Greenberg, M. E. (2004). Stress-Dependent Regulation of FOXO Transcription Factors by the SIRT1 Deacetylase. *Science*, *303*(5666), 2011–2015. https://doi.org/10.1126/science.1094637

Buwen, C., Cheng, L., Zhi, L., & Song, H. (2017). IOP Conference Series: Earth and Environmental Science Related content Research progress on trifluoromethyl-based radical reaction process. *IOP Conf. Ser.: Earth Environ. Sci*, *100*, 12061. https://doi.org/10.1088/1755-1315/100/1/012061

Cancer Today. (n.d.). Retrieved May 21, 2021, from https://gco.iarc.fr/today/online-analysis-table?v=2020&mode=cancer&mode_population=continents&population=900&populations=900&key=asr&sex=0&cancer=39&type=0&statistic=5&prevalence=0&population_group=0&ages_group%5B%5D=0&ages_group%5B%5D=17&group_cancer=1&include_nmsc=1&include_nmsc_other=1

Cea, M., Soncini, D., Fruscione, F., Raffaghello, L., Garuti, A., Emionite, L., Moran, E., Magnone, M., Zoppoli, G., Reverberi, D., Caffa, I., Salis, A., Cagnetta, A., Bergamaschi, M., Casciaro, S., Pierri, I., Damonte, G., Ansaldi, F., Gobbi, M., … Nencioni, A. (2011). Synergistic interactions between HDAC and sirtuin inhibitors in human leukemia cells. *PLoS ONE*, *6*(7), 22739. https://doi.org/10.1371/journal.pone.0022739

Chaitanya, G. V., Alexander, J. S., & Babu, P. P. (2010). PARP-1 cleavage fragments: Signatures of cell-death proteases in neurodegeneration. In *Cell Communication and Signaling* (Vol. 8). Cell Commun Signal. https://doi.org/10.1186/1478-811X-8-31

Chang, M. H., You, S. L., Chen, C. J., Liu, C. J., Lai, M. W., Wu, T. C., Wu, S. F., Lee, C. M., Yang, S. S., Chu, H. C., Wang, T. E., Chen, B. W., Chuang, W. L., Soon, M. S., Lin, C. Y., Chiou, S. T., Kuo, H. S., Chen, D. S., Yang, Y. J., … Cheng, Y. S. (2016). Long-term Effects of Hepatitis B Immunization of

Infants in Preventing Liver Cancer. *Gastroenterology*, *151*(3), 472-480.e1. https://doi.org/10.1053/j.gastro.2016.05.048

Chen, Q. W., Zhu, X. Y., Li, Y. Y., & Meng, Z. Q. (2014). Epigenetic regulation and cancer (review). In *Oncology Reports* (Vol. 31, Issue 2, pp. 523–532). Oncol Rep. https://doi.org/10.3892/or.2013.2913

Choi, H. N., Bae, J. S., Jamiyandorj, U., Noh, S. J., Park, H. S., Jang, K. Y., Chung, M. J., Kang, M. J., Lee, D. G., & Moon, W. S. (2011). Expression and role of SIRT1 in hepatocellular carcinoma. *Oncology Reports*, *26*(2), 503–510. https://doi.org/10.3892/or.2011.1301

CROssBAR Project. (n.d.). Retrieved August 4, 2021, from https://cansyl.metu.edu.tr/crossbar

Devi, N., Kaur, K., Biharee, A., & Jaitak, V. (2021). Recent Development in Indole Derivatives as Anticancer Agent: A Mechanistic Approach. *Anti-Cancer Agents in Medicinal Chemistry*, *21*. https://doi.org/10.2174/1871520621999210104192644

El-Serag, H. B. (2011). Hepatocellular Carcinoma. *New England Journal of Medicine*, *365*(12), 1118–1127. https://doi.org/10.1056/NEJMra1001683

Farcas, M., Gavrea, A. A., Gulei, D., Ionescu, C., Irimie, A., Catana, C. S., & Berindan-Neagoe, I. (2019). SIRT1 in the Development and Treatment of Hepatocellular Carcinoma. In *Frontiers in Nutrition* (Vol. 6, p. 148). Frontiers Media S.A. https://doi.org/10.3389/fnut.2019.00148

H, Y., K, B., N, O., S, S., E, C., A, T., N, T., M, Y., E, E., KC, A., N, A., & M, O. (2009). Canonical Wnt signaling is antagonized by noncanonical Wnt5a in hepatocellular carcinoma cells. *Molecular Cancer*, *8*, 90. https://doi.org/10.1186/1476-4598-8-90

Hao, C., Zhu, P. X., Yang, X., Han, Z. P., Jiang, J. H., Zong, C., Zhang, X. G., Liu, W. T., Zhao, Q. D., Fan, T. T., Zhang, L., & Wei, L. X. (2014).

Overexpression of SIRT1 promotes metastasis through epithelial-mesenchymal transition in hepatocellular carcinoma. *BMC Cancer*, *14*(1), 1–10. https://doi.org/10.1186/1471-2407-14-978

Hawash, M., Kahraman, D. C., Cetin-Atalay, R., & Baytas, S. N. (2021). Induction of Apoptosis in Hepatocellular Carcinoma Cell Lines by Novel Indolylacrylamide Derivatives: Synthesis and Biological Evaluation. *Chemistry and Biodiversity*, *18*(5), e2001037. https://doi.org/10.1002/cbdv.202001037

Heltweg, B., Gatbonton, T., Schuler, A. D., Posakony, J., Li, H., Goehle, S., Kollipara, R., DePinho, R. A., Gu, Y., Simon, J. A., & Bedalov, A. (2006). Antitumor activity of a small-molecule inhibitor of human silent information regulator 2 enzymes. *Cancer Research*, *66*(8), 4368–4377. https://doi.org/10.1158/0008-5472.CAN-05-3617

Ho, D. W. H., Lo, R. C. L., Chan, L. K., & Ng, I. O. L. (2016). Molecular pathogenesis of hepatocellular carcinoma. In *Liver Cancer* (Vol. 5, Issue 4, pp. 290–302). S. Karger AG. https://doi.org/10.1159/000449340

Hu, J., Jing, H., & Lin, H. (2014). Sirtuin inhibitors as anticancer agents. In *Future Medicinal Chemistry* (Vol. 6, Issue 8, pp. 945–966). Future Science. https://doi.org/10.4155/fmc.14.44

In fight against cancer, a closer look at nuclear blebbing -- ScienceDaily. (n.d.). Retrieved May 21, 2021, from https://www.sciencedaily.com/releases/2013/02/130219121606.htm

Jeong, J., Juhn, K., Lee, H., Kim, S. H., Min, B. H., Lee, K. M., Cho, M. H., Park, G. H., & Lee, K. H. (2007). SIRT1 promotes DNA repair activity and deacetylation of Ku70. *Experimental and Molecular Medicine*, *39*(1), 8–13. https://doi.org/10.1038/emm.2007.2

Jung-Hynes, B., Nihal, M., Zhong, W., & Ahmad, N. (2009). Role of sirtuin histone deacetylase SIRT1 in prostate cancer: A target for prostate cancer

management via its inhibition? *Journal of Biological Chemistry*, *284*(6), 3823–3832. https://doi.org/10.1074/jbc.M807869200

Kan, Z., Zheng, H., Liu, X., Li, S., Barber, T. D., Gong, Z., Gao, H., Hao, K., Willard, M. D., Xu, J., Hauptschein, R., Rejto, P. A., Fernandez, J., Wang, G., Zhang, Q., Wang, B., Chen, R., Wang, J., Lee, N. P., … Mao, M. (n.d.). *Whole-genome sequencing identifies recurrent mutations in hepatocellular carcinoma*. https://doi.org/10.1101/gr.154492.113

Kim, H. S., Patel, K., Muldoon-Jacobs, K., Bisht, K. S., Aykin-Burns, N., Pennington, J. D., van der Meer, R., Nguyen, P., Savage, J., Owens, K. M., Vassilopoulos, A., Ozden, O., Park, S. H., Singh, K. K., Abdulkadir, S. A., Spitz, D. R., Deng, C. X., & Gius, D. (2010). SIRT3 Is a Mitochondria-Localized Tumor Suppressor Required for Maintenance of Mitochondrial Integrity and Metabolism during Stress. *Cancer Cell*, *17*(1), 41–52. https://doi.org/10.1016/j.ccr.2009.11.023

Lau, C. C., Sun, T., Ching, A. K. K., He, M., Li, J. W., Wong, A. M., Co, N. N., Chan, A. W. H., Li, P. S., Lung, R. W. M., Tong, J. H. M., Lai, P. B. S., Chan, H. L. Y., To, K. F., Chan, T. F., & Wong, N. (2014). Viral-human chimeric transcript predisposes risk to liver cancer development and progression. *Cancer Cell*, *25*(3), 335–349. https://doi.org/10.1016/j.ccr.2014.01.030

Lee, C. W., Wong, L. L. Y., Tse, E. Y. T., Liu, H. F., Leong, V. Y. L., Lee, J. M. F., Hardie, D. G., Ng, I. O. L., & Ching, Y. P. (2012). AMPK promotes p53 acetylation via phosphorylation and inactivation of SIRT1 in liver cancer cells. *Cancer Research*, *72*(17), 4394–4404. https://doi.org/10.1158/0008-5472.CAN-12-0429

Li, Y., Xu, S., Li, J., Zheng, L., Feng, M., Wang, X., Han, K., Pi, H., Li, M., Huang, X., You, N., Tian, Y., Zuo, G., Li, H., Zhao, H., Deng, P., Yu, Z., Zhou, Z., & Liang, P. (2016). SIRT1 facilitates hepatocellular carcinoma metastasis by promoting PGC-1α-mediated mitochondrial biogenesis.

Oncotarget, *7*(20), 29255–29274. https://doi.org/10.18632/oncotarget.8711

Lin, X. lin, Li, K., Yang, Z., Chen, B., & Zhang, T. (2020). Dulcitol suppresses proliferation and migration of hepatocellular carcinoma via regulating SIRT1/p53 pathway. *Phytomedicine*, *66*, 153112. https://doi.org/10.1016/j.phymed.2019.153112

Liou, G. G., Tanny, J. C., Kruger, R. G., Walz, T., & Moazed, D. (2005). Assembly of the SIR complex and its regulation by O-acetyl-ADP-ribose, a product of NAD-dependent histone deacetylation. *Cell*, *121*(4), 515–527. https://doi.org/10.1016/j.cell.2005.03.035

Liu, Y., Chang, C. C. H., Marsh, G. M., & Wu, F. (2012). Population attributable risk of aflatoxin-related liver cancer: Systematic review and meta-analysis. *European Journal of Cancer*, *48*(14), 2125–2136. https://doi.org/10.1016/j.ejca.2012.02.009

Ma, L., Chua, M. S., Andrisani, O., & So, S. (2014). Epigenetics in hepatocellular carcinoma: An update and future therapy perspectives. In *World Journal of Gastroenterology* (Vol. 20, Issue 2, pp. 333–345). Baishideng Publishing Group Co. https://doi.org/10.3748/wjg.v20.i2.333

Malmstrom, R. D., & Watowich, S. J. (2011). Using free energy of binding calculations to improve the accuracy of virtual screening predictions. *Journal of Chemical Information and Modeling*, *51*(7), 1648–1655. https://doi.org/10.1021/ci200126v

Mao, B., Hu, F., Cheng, J., Wang, P., Xu, M., Yuan, F., Meng, S., Wang, Y., Yuan, Z., & Bi, W. (2014). SIRT1 regulates YAP2-mediated cell proliferation and chemoresistance in hepatocellular carcinoma. *Oncogene*, *33*, 1468–1474. https://doi.org/10.1038/onc.2013.88

Martins, P., Jesus, J., Santos, S., Raposo, L. R., Roma-Rodrigues, C., Baptista, P. V., & Fernandes, A. R. (2015). Heterocyclic anticancer compounds: Recent advances and the paradigm shift towards the use of nanomedicine's tool Box.

In *Molecules* (Vol. 20, Issue 9, pp. 16852–16891). MDPI AG. https://doi.org/10.3390/molecules200916852

Mcglynn, K. A., Petrick, J. L., & London, W. T. (n.d.). *Global epidemiology of hepatocellular carcinoma: an emphasis on demographic and regional variability*. https://doi.org/10.1016/j.cld.2015.01.001

Moeini, A., Cornellà, H., & Villanueva, A. (2012). Emerging Signaling Pathways in Hepatocellular Carcinoma. *Liver Cancer*, *1*(2), 83–93. https://doi.org/10.1159/000342405

Morris, G. M., Ruth, H., Lindstrom, W., Sanner, M. F., Belew, R. K., Goodsell, D. S., & Olson, A. J. (2009). Software news and updates AutoDock4 and AutoDockTools4: Automated docking with selective receptor flexibility. *Journal of Computational Chemistry*, *30*(16), 2785–2791. https://doi.org/10.1002/jcc.21256

Nault, J. C., Mallet, M., Pilati, C., Calderaro, J., Bioulac-Sage, P., Laurent, C., Laurent, A., Cherqui, D., Balabaud, C., & Zucman-Rossi, J. (2013). *ARTICLE High frequency of telomerase reverse-transcriptase promoter somatic mutations in hepatocellular carcinoma and preneoplastic lesions*. https://doi.org/10.1038/ncomms3218

Osborne, B., Cooney, G. J., & Turner, N. (2014). Are sirtuin deacylase enzymes important modulators of mitochondrial energy metabolism? In *Biochimica et Biophysica Acta - General Subjects* (Vol. 1840, Issue 4, pp. 1295–1302). Elsevier. https://doi.org/10.1016/j.bbagen.2013.08.016

Palmirotta, R., Cives, M., Della-Morte, D., Capuani, B., Lauro, D., Guadagni, F., & Silvestris, F. (2016). Sirtuins and Cancer: Role in the Epithelial-Mesenchymal Transition. In *Oxidative Medicine and Cellular Longevity* (Vol. 2016). Hindawi Publishing Corporation. https://doi.org/10.1155/2016/3031459

Park, J. W., Chen, M., Colombo, M., Roberts, L. R., Schwartz, M., Chen, P. J., Kudo, M., Johnson, P., Wagner, S., Orsini, L. S., & Sherman, M. (2015).

Global patterns of hepatocellular carcinoma management from diagnosis to death: The BRIDGE Study. *Liver International*, *35*(9), 2155–2166. https://doi.org/10.1111/liv.12818

Park, S. Y., Lee, K. B., Lee, M. J., Bae, S. C., & Jang, J. J. (2012). Nicotinamide inhibits the early stage of carcinogen-induced hepatocarcinogenesis in mice and suppresses human hepatocellular carcinoma cell growth. *Journal of Cellular Physiology*, *227*(3), 899–908. https://doi.org/10.1002/jcp.22799

Patel, N. S., Hooker, J., Gonzalez, M., Bhatt, A., Nguyen, P., Ramirez, K., Richards, L., Rizo, E., Hernandez, C., Kisseleva, T., Schnabl, B., Brenner, D., Sirlin, C. B., & Loomba, R. (2017). Weight Loss Decreases Magnetic Resonance Elastography Estimated Liver Stiffness in Nonalcoholic Fatty Liver Disease. In *Clinical Gastroenterology and Hepatology* (Vol. 15, Issue 3, pp. 463–464). W.B. Saunders. https://doi.org/10.1016/j.cgh.2016.09.150

Portmann, S., Fahrner, R., Lechleiter, A., Keogh, A., Overney, S., Laemmle, A., Mikami, K., Montani, M., Tschan, M. P., Candinas, D., & Stroka, D. (2013). Antitumor effect of SIRT1 inhibition in human HCC tumor models in vitro and in vivo. *Molecular Cancer Therapeutics*, *12*(4), 499–508. https://doi.org/10.1158/1535-7163.MCT-12-0700

R, L., A, W., B, P., E, F., M, P., F, L., O, D. W., & P, P. (2012). Comparative analysis of dynamic cell viability, migration and invasion assessments by novel real-time technology and classic endpoint assays. *PloS One*, *7*(10). https://doi.org/10.1371/JOURNAL.PONE.0046536

Rifaioglu, A. S., Nalbat, E., Atalay, V., Martin, M. J., Cetin-Atalay, R., & Doğan, T. (2020). DEEPScreen: high performance drug-target interaction prediction with convolutional neural networks using 2-D structural compound representations. *Chemical Science*, *11*(9), 2531–2557. https://doi.org/10.1039/c9sc03414e

Sachdeva, H., Mathur, J., & Guleria, A. (2020). Indole derivatives as potential

anticancer agents: A review. *Journal of the Chilean Chemical Society*, *65*(3), 4900–4907. https://doi.org/10.4067/s0717-97072020000204900

Sakai, T., Matsumoto, Y., Ishikawa, M., Sugita, K., Hashimoto, Y., Wakai, N., Kitao, A., Morishita, E., Toyoshima, C., Hayashi, T., & Akiyama, T. (2015). Design, synthesis and structure-activity relationship studies of novel sirtuin 2 (SIRT2) inhibitors with a benzamide skeleton. *Bioorganic and Medicinal Chemistry*, *23*(2), 328–339. https://doi.org/10.1016/j.bmc.2014.11.027

Sarveazad, A., Agah, S., Babahajian, A., Amini, N., & Bahardoust, M. (2019). Predictors of 5 year survival rate in hepatocellular carcinoma patients. *Journal of Research in Medical Sciences | Published by Wolters Kluwer-Medknow*, *1*. https://doi.org/10.4103/jrms.JRMS_1017_18

Schilling, T., Kairat, A., Melino, G., Krammer, P. H., Stremmel, W., Oren, M., & Müller, M. (2010). Interference with the p53 family network contributes to the gain of oncogenic function of mutant p53 in hepatocellular carcinoma. *Biochemical and Biophysical Research Communications*, *394*(3), 817–823. https://doi.org/10.1016/J.BBRC.2010.03.082

Schulze, K., Imbeaud, S., Letouzé, E., Alexandrov, L. B., Calderaro, J., Rebouissou, S., Couchy, G., Meiller, C., Shinde, J., Soysouvanh, F., Calatayud, A.-L., Pinyol, R., Pelletier, L., Balabaud, C., Laurent, A., Blanc, J.-F., Mazzaferro, V., Calvo, F., Villanueva, A., … Zucman-Rossi, J. (2015). Exome sequencing of hepatocellular carcinomas identifies new mutational signatures and potential therapeutic targets Europe PMC Funders Group. *Nat Genet*, *47*(5), 505–511. https://doi.org/10.1038/ng.3252

Sharma, S., Kelly, T. K., & Jones, P. A. (2009). Epigenetics in cancer. In *Carcinogenesis* (Vol. 31, Issue 1, pp. 27–36). Carcinogenesis. https://doi.org/10.1093/carcin/bgp220

Someya, S., Yu, W., Hallows, W. C., Xu, J., Vann, J. M., Leeuwenburgh, C., Tanokura, M., Denu, J. M., & Prolla, T. A. (2010). Sirt3 mediates reduction of

oxidative damage and prevention of age-related hearing loss under Caloric Restriction. *Cell*, *143*(5), 802–812. https://doi.org/10.1016/j.cell.2010.10.002

Sravanthi, T. V., & Manju, S. L. (2016). Indoles - A promising scaffold for drug development. In *European Journal of Pharmaceutical Sciences* (Vol. 91, pp. 1–10). Elsevier B.V. https://doi.org/10.1016/j.ejps.2016.05.025

Tanno, M., Sakamoto, J., Miura, T., Shimamoto, K., & Horio, Y. (2007). Nucleocytoplasmic shuttling of the NAD+-dependent histone deacetylase SIRT1. *Journal of Biological Chemistry*, *282*(9), 6823–6832. https://doi.org/10.1074/jbc.M609554200

Totoki, Y., Tatsuno, K., Covington, K. R., Ueda, H., Creighton, C. J., Kato, M., Tsuji, S., Donehower, L. A., Slagle, B. L., Nakamura, H., Yamamoto, S., Shinbrot, E., Hama, N., Lehmkuhl, M., Hosoda, F., Arai, Y., Walker, K., Dahdouli, M., Gotoh, K., … Shibata, T. (2014). Trans-ancestry mutational landscape of hepatocellular carcinoma genomes. *Nature GeNetics VOLUME*, *46*. https://doi.org/10.1038/ng.3126

Vaquero, A., Scher, M. B., Dong, H. L., Sutton, A., Cheng, H. L., Alt, F. W., Serrano, L., Sternglanz, R., & Reinberg, D. (2006). SirT2 is a histone deacetylase with preference for histone H4 Lys 16 during mitosis. *Genes and Development*, *20*(10), 1256–1261. https://doi.org/10.1101/gad.1412706

Wang, S., Cheng, L., Liu, Y., Wang, J., & Jiang, W. (2016). Indole-3-Carbinol (I3C) and its Major Derivatives: Their Pharmacokinetics and Important Roles in Hepatic Protection. *Current Drug Metabolism*, *17*(4), 401–409. https://doi.org/10.2174/1389200217666151210125105

Wang, Y., He, J., Liao, M., Hu, M., Li, W., Ouyang, H., Wang, X., Ye, T., Zhang, Y., & Ouyang, L. (2019). An overview of Sirtuins as potential therapeutic target: Structure, function and modulators. In *European Journal of Medicinal Chemistry* (Vol. 161, pp. 48–77). Elsevier Masson s.r.l. https://doi.org/10.1016/j.ejmech.2018.10.028

Whittaker, S., Marais, R., & Zhu, A. X. (2010). The role of signaling pathways in the development and treatment of hepatocellular carcinoma. *Oncogene*, *29*(36), 4989–5005. https://doi.org/10.1038/onc.2010.236

Wu, D., Rice, C. M., & Wang, X. (2012). Cancer bioinformatics: A new approach to systems clinical medicine. *BMC Bioinformatics*, *13*(1), 71. https://doi.org/10.1186/1471-2105-13-71

Wu, X., & Li, Y. (2012). Signaling Pathways in Liver Cancer. In *Liver Tumors*. InTech. https://doi.org/10.5772/31381

Yanagisawa, S., Baker, J. R., Vuppusetty, C., Koga, T., Colley, T., Fenwick, P., Donnelly, L. E., Barnes, P. J., & Ito, K. (2018). The dynamic shuttling of SIRT1 between cytoplasm and nuclei in bronchial epithelial cells by single and repeated cigarette smoke exposure. *PLoS ONE*, *13*(3). https://doi.org/10.1371/journal.pone.0193921

Yang, J. D., Hainaut, P., Gores, G. J., Amadou, A., Plymoth, A., & Roberts, L. R. (2019). A global view of hepatocellular carcinoma: trends, risk, prevention and management. *Nature Reviews Gastroenterology and Hepatology*, *16*(10), 589–604. https://doi.org/10.1038/s41575-019-0186-y

Yeung, F., Hoberg, J. E., Ramsey, C. S., Keller, M. D., Jones, D. R., Frye, R. A., & Mayo, M. W. (2004). Modulation of NF-κB-dependent transcription and cell survival by the SIRT1 deacetylase. *EMBO Journal*, *23*(12), 2369–2380. https://doi.org/10.1038/sj.emboj.7600244

APPENDICES-1

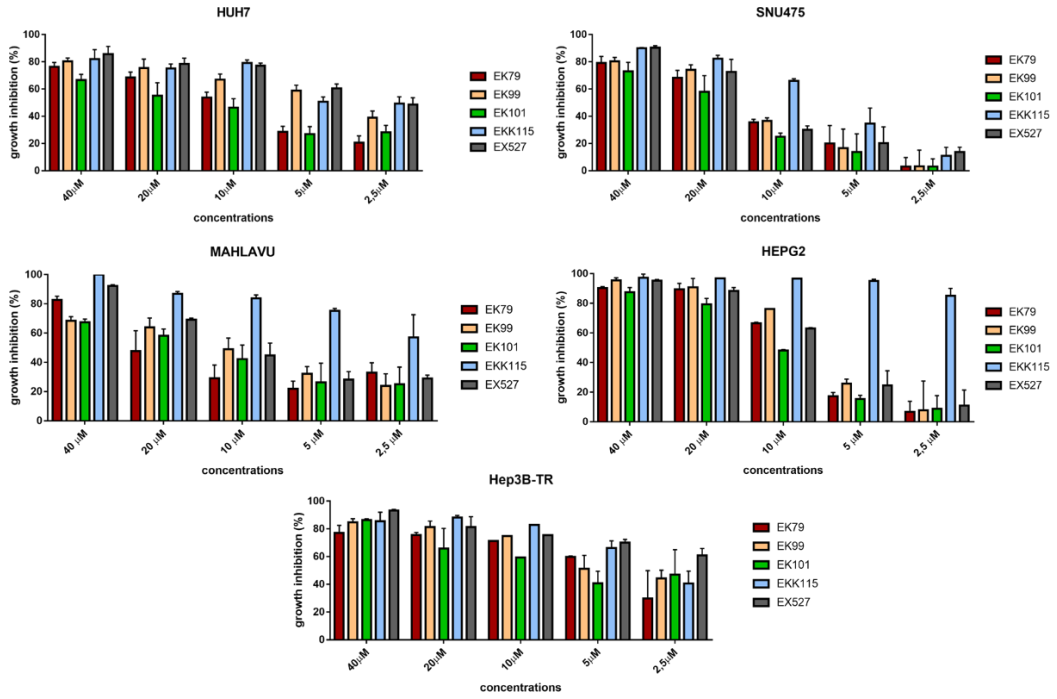

Supplementary Figure 1: Growth inhibition capacity of the molecules in the HCC cells. Cells were treated with 40, 20, 10, 5, and 2,5 µM of the molecules for 72 hours. Then the growth inhibition was calculated by the normalization to the DMSO group.

APPENDICES-2

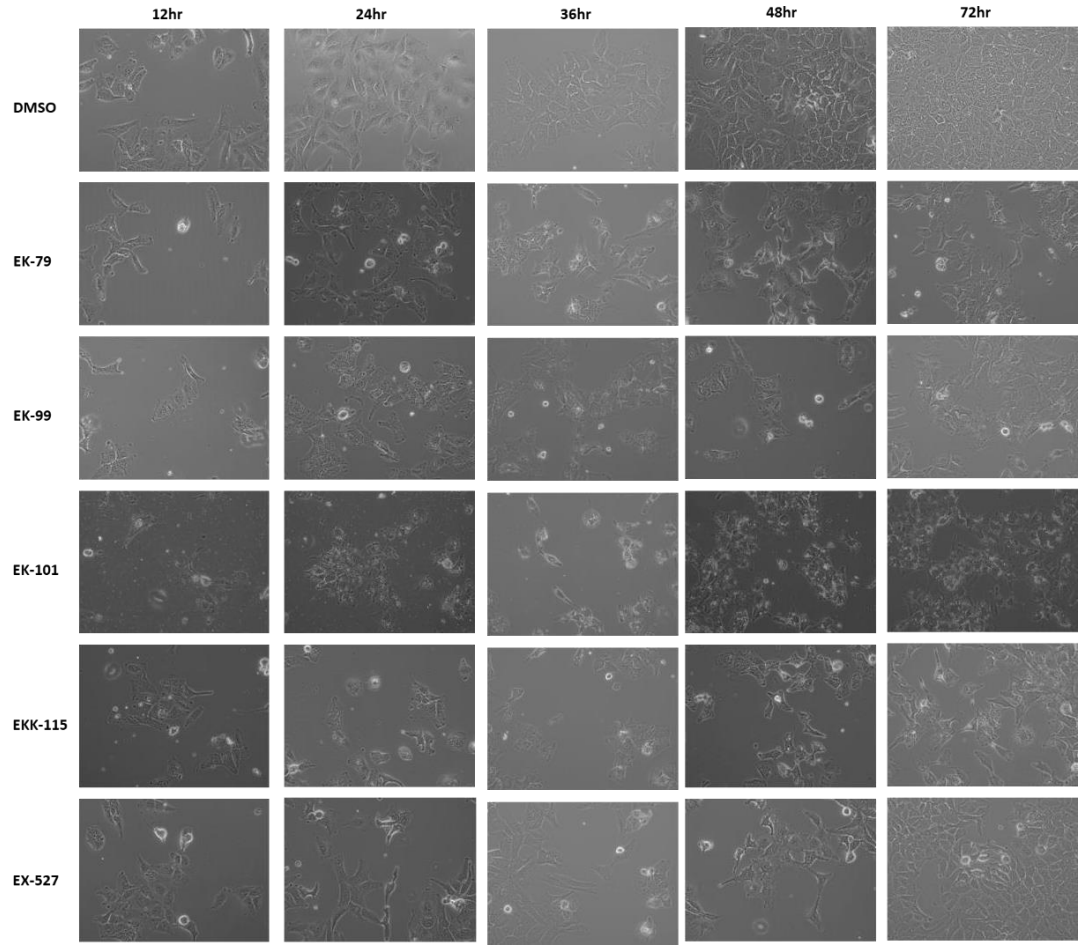

Supplementary Figure 2: The time-course observation of Huh7 cells upon the molecule treatment. The cells were treated with IC_{100} concentration of the molecules for 12, 24, 26, 48, and 72 hours. Images were taken by light microscopy with 20 X magnification.

APPENDICES-3

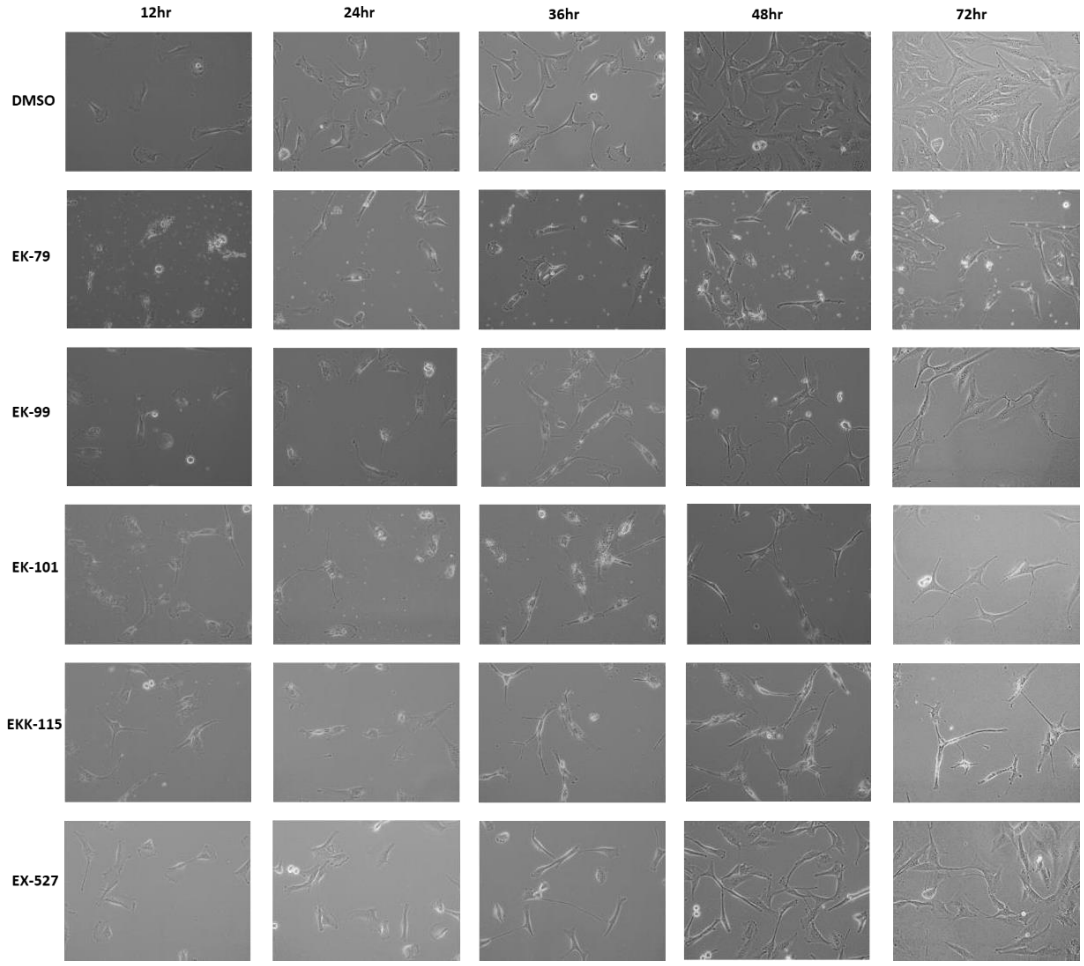

Supplementary Figure 3: The time-course observation of SNU475 cells upon the molecule treatment. The cells were treated with IC_{100} concentration of the molecules for 12, 24, 26, 48, and 72 hours. Images were taken by light microscopy with 20 X magnification.

APPENDICES-4

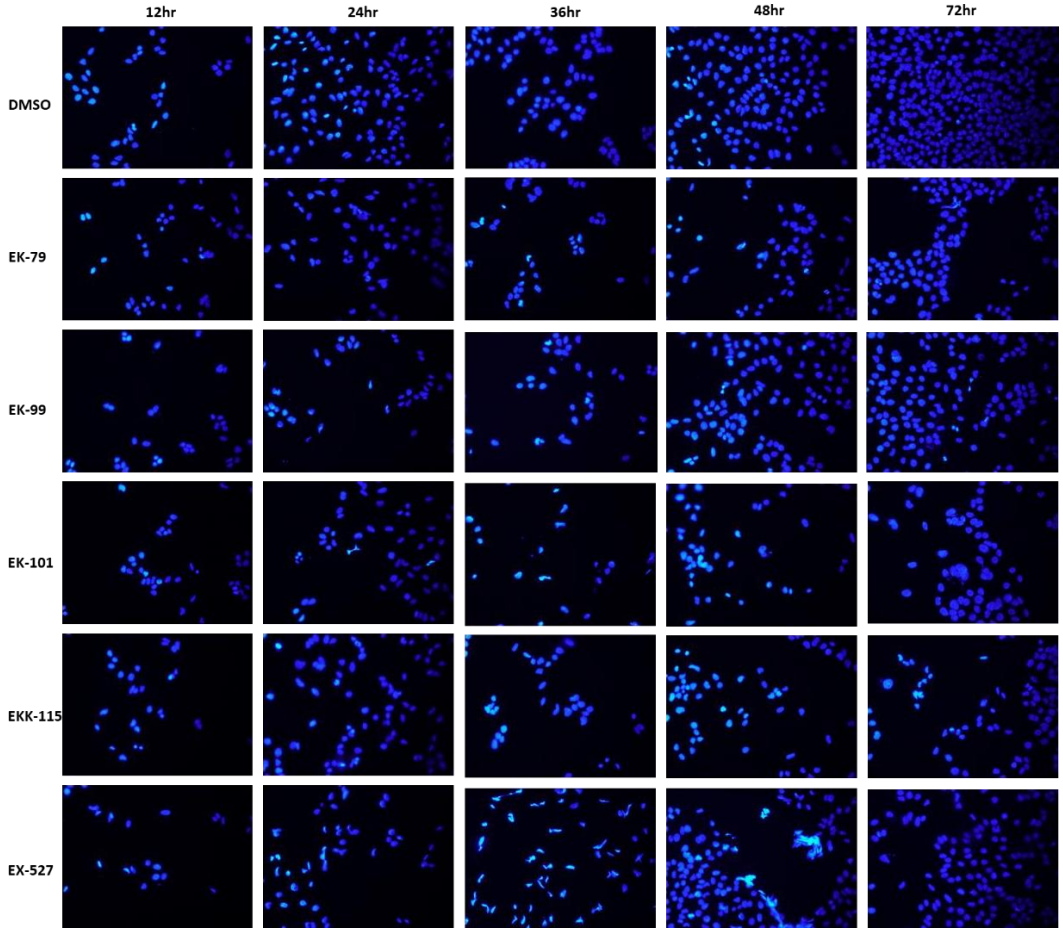

Supplementary Figure 4: Hoechst staining of Huh7 cells in time course. The cells were treated with IC_{100} concentration of the molecules for 12, 24, 26, 48, and 72 hours. Images were taken by fluorescent microscopy with 20 X magnification.

APPENDICES-5

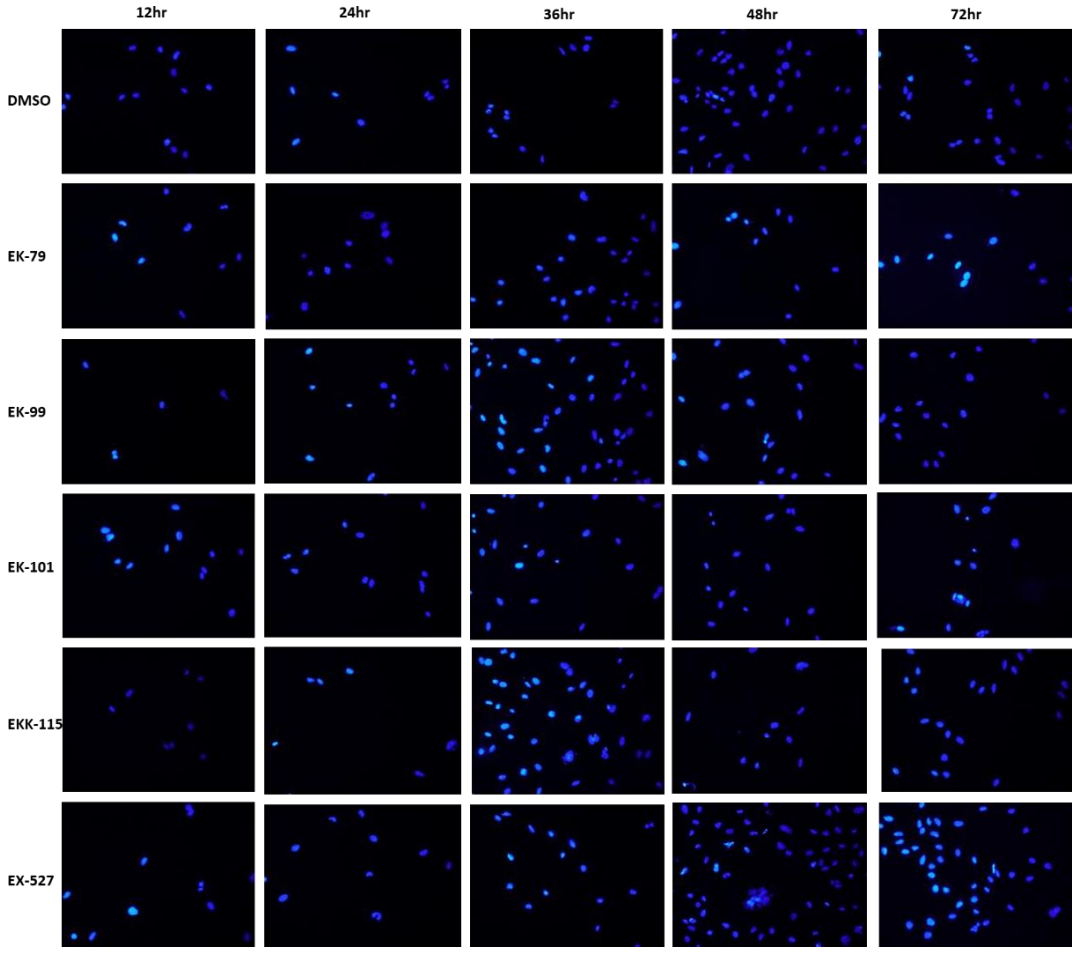

Supplementary Figure 5: Hoechst staining of SNU475 cells in time course. The cells were treated with IC_{100} concentration of the molecules for 12, 24, 26, 48, and 72 hours. Images were taken by fluorescent microscopy with 20 X magnification.

APPENDICES-6

COPYRIGHT FOR FIGURE 1.1

SPRINGER NATURE LICENSE TERMS AND CONDITIONS

Aug 11, 2021

This Agreement between Miss. Büşra Bınarcı ("You") and Springer Nature ("Springer Nature") consists of your license details and the terms and conditions provided by

Springer Nature and Copyright Clearance Center.

License Number: 5125921445891

License date: Aug 11, 2021

Licensed Content Publisher: Springer Nature

Licensed Content Publication: Oncogene

Licensed Content Title: The role of signaling pathways in the development and treatment of hepatocellular carcinoma

Licensed Content Author : S Whittaker et al

Licensed Content Date: Jul 19, 2010

Type of Use: Thesis/Dissertation

Requestor type: non-commercial (non-profit)

Format: print and electronic

Portion: figures/tables/illustrations

Number of figures/tables/illustrations: 1

High-res required: no

Will you be translating?: no

Circulation/distribution: 1 - 29

Author of this Springer Nature content

Title: BIOACTIVITY ANALYSIS OF NOVEL INDOLE

DERIVATIVES ON HEPATOCELLULAR CARCINOMA AS SIRTUIN INHIBITORS

Institution name: Middle East Technical University

Expected presentation date: Sep 2021

Order reference number :Copyright for Figure 1.1

Portions: Figure 2

Requestor Location

Miss. Büşra Bınarcı

Middle East Technical University Department of Biology

Room 223

Ankara, Çankaya 06800 Turkey

Attn: Miss. Büşra Bınarcı

Total 0.00 USD

APPENDICES-7

COPYRIGHT FOR FIGURE 1.4.1

ELSEVIER LICENSE TERMS AND CONDITIONS

Aug 11, 2021

This Agreement between Miss. Büşra Bınarcı ("You") and Elsevier ("Elsevier") consists of your license details and the terms and conditions provided by Elsevier and Copyright Clearance Center.

License Number: 5125930560322

License date: Aug 11, 2021

Licensed Content Publisher: Elsevier

Licensed Content Publication: Drug Resistance Updates

Licensed Content Title: Interplay between SIRT proteins and tumour suppressor transcription factors in chemotherapeutic resistance of cancer

Licensed Content Author: Yolanda Olmos,Jan J. Brosens,Eric W.-F. Lam

Licensed Content Date: Feb 1, 2011

Licensed Content Volume

Licensed Content Issue: 1

Licensed Content Pages:10 Start Page: 35 End Page: 44

Type of Use: reuse in a thesis/dissertation

Portion: figures/tables/illustrations

Number of 1 figures/tables/illustrations

Format: both print and electronic

Are you the author of this Elsevier article?: no

Will you be translating?: No

Title: BIOACTIVITY ANALYSIS OF NOVEL INDOLE DERIVATIVES ON HEPATOCELLULAR CARCINOMA AS SIRTUIN INHIBITORS

Institution name: Middle East Technical University

Expected presentation date: Sep 2021

Order reference number: copyright for Figure 1.4.1

Portions: Figure 3

Requestor Location

Miss. Büşra Bınarcı

Middle East Technical University Department of Biology

Room 223

Ankara, Çankaya 06800 Turkey

Attn: Miss. Büşra Bınarcı

Publisher Tax ID GB 494 6272 12

Total 0.00 USD

APPENDICES-8

COPYRIGHT FOR FIGURE 1.4.2

ELSEVIER LICENSE TERMS AND CONDITIONS

Aug 11, 2021

This Agreement between Miss. Büşra Bınarcı ("You") and Elsevier ("Elsevier") consists of your license details and the terms and conditions provided by Elsevier and Copyright Clearance Center.

License Number: 5125930768604

License date: Aug 11, 2021

Licensed Content Publisher: Elsevier

Licensed Content Publication: Phytomedicine

Licensed Content Title: Dulcitol suppresses proliferation and migration of hepatocellular carcinoma via regulating SIRT1/p53 pathway

Licensed Content Author: Xiao lin Lin,Kai Li,Zhuo Yang,Baogui Chen,Tao Zhang

Licensed Content Date: Jan 1, 2020

Type of Use: reuse in a thesis/dissertation

Portion: figures/tables/illustrations

Number of 1 figures/tables/illustrations

Format: both print and electronic

Are you the author of this Elsevier article? No

Will you be translating? No

Title: BIOACTIVITY ANALYSIS OF NOVEL INDOLE DERIVATIVES ON

HEPATOCELLULAR CARCINOMA AS SIRTUIN INHIBITORS

Institution name: Middle East Technical University

Expected presentation date: Sep 2021

Order reference number: copyright for figure 1.4.2

Portions: Graphical abstract

Requestor Location

Miss. Büşra Bınarcı

Middle East Technical University Department of Biology

Room 223

Ankara, Çankaya 06800 Turkey

Attn: Miss. Büşra Bınarcı

Publisher Tax ID GB 494 6272 12

Total 0.00 USD